Corrections to dynamic scaling for the λ transition in liquid helium. II. Quasiscaling

Richard A. Ferrell and Jayanta K. Bhattacharjee*
Center for Theoretical Physics of the Department of Physics and Astronomy, University of Maryland, College Park, Maryland 20742
(Received 27 December 1982)

We give a general phenomenological treatment of the crossover of the critical dynamics from background to the asymptotic region. The log-log plot of the entropy diffusion coefficient versus wave number exhibits a point of inflexion in the crossover region. The resulting straight portion of the curve produces "quasiscaling," with an apparent critical exponent 18% bigger than expected from dynamic scaling. Our $\vec{k}$-space treatment of the crossover has some advantages over the conventional renormalization-group method. By evaluating the loop integrals in three dimensions we furthermore are able to impose rigorous conditions on the precritical rise.

I. INTRODUCTION

In this paper we return to a problem that we consider to have solved more than three years ago in four papers, Refs. 1–4. In the interim, various workers[5–8] have questioned the validity of our solution. For this reason we present here the complete background for our treatment of the corrections to scaling at the λ point in liquid helium. Our purpose is to render the full account in great detail so that all readers will be able to understand our approach. Our basic philosophy is to use two-loop mode coupling as a qualitative guide, but not to rely on it as a quantitative computational tool. We believe that the other work that has been done on this problem since our publications, such as the detailed differential renormalization-group computations of Dohm and Folk,[7] is a positive contribution to the field insofar as it indicates general features that can be expected to be insensitive to the shortcomings of the truncated loop expansion. But we are doubtful of claims of high numerical accuracy because of the limitation of these calculations to two loops. Our method is different. We exploit the two-loop truncation of the loop expansion to set up an appropriate phenomenology, which we then employ for the calculation. What do we calculate? To answer briefly, *one number.* Here, again, our emphasis is primarily on the important gross features. To summarize our results, we find a "quasiscaling" region in which there is effectively scaling, but with an effective critical exponent increased by the factor $1+z_Q$. Thus our main quantitative result is a value for z_Q, the quasiscaling exponent. The value of z_Q that we find is a confirmation of what we reported before[1]—namely, $z_Q \simeq 0.2$, corresponding to an apparent 20% increase in the strength of the critical divergence exponent. We feel that this limitation of the ambitions of the theory to the calculation of one number is appropriate at the present time, given both the shortcomings of the theory and the confused experimental situation.[8]

In the λ transition of liquid ^{4}He we are dealing with the rates $\gamma_{S,\psi}$ of relaxation of fluctuations of the entropy (S) and order parameter (ψ). For self-consistency[4] these rates are evaluated at the frequency $i\gamma_\psi$. The fluctuations influence one another, and we need to know $\gamma_{S,\psi}$ in the whole k-κ plane (wave number and reciprocal correlation length) shown in Fig. 1. We restrict ourselves here to the behavior along the k axis ($\kappa=0$) and study all of the relevant functions as a function of wave number only. This simplifies the problem considerably because then we do not need scaling functions for $\gamma_{S,\psi}$. In other words, $\gamma_{S,\psi}$ are functions of only one variable rather than two. It is convenient to introduce the kinetic coefficients

$$D_{S,\psi}(k)=\frac{1}{k^2}\gamma_{S,\psi}(k)\ , \tag{1.1}$$

which take on the noncritical background values $B_{S,\psi}$ for sufficiently large k, as shown by the outer region in Fig. 1. Decreasing k brings us into the "van Hove" or "precritical region."[2,3,9] As shown by the dotted-dashed curve in Fig. 2, this first appearance of critical behavior in D_S or D_ψ is a "precritical rise" which is proportional to k^{-1}. It is readily calculated by a single-loop integral.[2,3] The single-loop integral needs, however, to be augmented by a two-loop correction[10] as k is further decreased. Additional corrections and higher-order effects need to be taken into

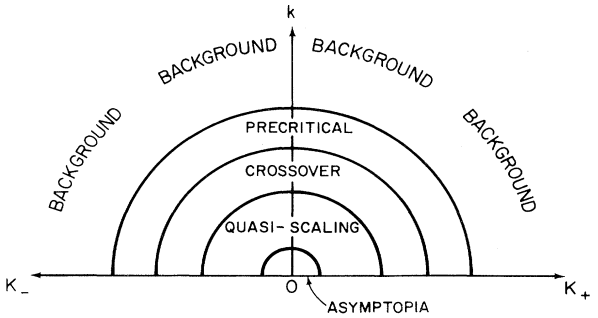

FIG. 1. Regions of wave-number space. $\kappa_\pm$ are the reciprocal correlation lengths above and below the λ point, respectively. We work at the λ point, where $\kappa_+=\kappa_-=0$, and study the dependence of the kinetic coefficients on the wave number k. "Asymptopia" and the background and precritical regions are the "anchor" regions for the interpolation through the intermediate crossover and quasiscaling regions.

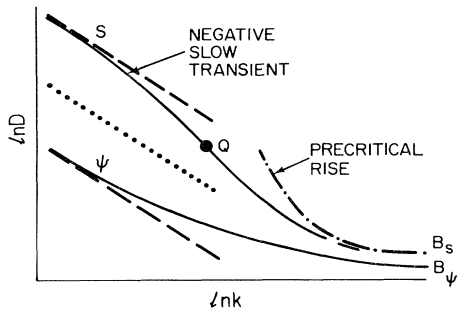

FIG. 2. Origin of the quasiscaling point. The entropy (S) and order-parameter (ψ) kinetic coefficients $D_{S,\psi}$ (dashed lines) differ by a large factor $w^* \gg 1$ in the asymptotic region (left end) but by the small factor $w_B^{-1} = B_S/B_\psi$ in the noncritical background region (right end). Matching D_S to its precritical rise requires a negative slow transient. The resulting point of inflexion (Q) produces quasiscaling in its vicinity.

account in the "crossover" region. The problem, however, simplifies again in the quasiscaling region, where D_S scales according to $k^{-(1+z_Q)/2}$. These nested regions are illustrated by the concentric rings in Fig. 1. As already mentioned, the study and parametrization of the quasiscaling behavior are the main objective of this paper. Finally, if it exists at all, the true asymptotic scaling region is restricted to an extremely small interval of k space near $k=0$, as indicated by the small semicircle in the center of Fig. 1. For this reason the asymptotic region is expected to have no direct practical importance except insofar as it influences the quasiscaling behavior. The latter, translated to the horizontal axis of Fig. 1, yields a thermodynamic ($k=0$) dependence $D_S \propto \kappa^{-(1+z_Q)/2}$. The exact numerical coefficient, which we do not attempt to calculate here, depends upon the scaling function. As mentioned above, we restrict ourselves almost exclusively in this paper to the vertical axis ($\kappa=0$) of Fig. 1.

Figure 2 is a schematic representation of the k dependence of $D_{S,\psi}$. The dashed straight lines represent the scaling solution

$$D_{S,\psi}(k) = a_{S,\psi} k^{-1/2} \tag{1.2}$$

(under the assumption that there does exist an asymptotic scaling region). By Eq. (1.2) both of these lines have the same slope on the log-log plot. But because of the small fixed-point value[11,12,4] of the ratio

$$w^* = \frac{a_\psi}{a_S} , \tag{1.3}$$

the scaling lines are widely separated. The dotted line shows the k dependence that would be expected for D_S and D_ψ if this special effect did not occur and a_ψ were equal to a_S. In fact, as shown in Sec. III below, D_ψ and D_S do have approximately the same precritical rise above their background values $B_{\psi,S}$. However, as illustrated in Fig. 2 by the solid curves, as k decreases the ratio D_S/D_ψ grows from its background value w_B^{-1} to its very much larger fixed-point value w^{*-1}. This gradual splitting apart of the curves is described by the slow transient, as discussed in Sec. 5.2 of Ref. 4. The essential point in Ref. 1 was that the coefficient of the slow transient in D_S is *negative*. This is necessary in order that, for increasing k, D_S should drop below the scaling line and match onto the relatively lower precritical curve at the larger values of k. Because of the negative amplitude of the slow transient, it is inescapable that a large portion of the D_S curve should be steeper than the scaling line, as described by

$$1 + z_{\text{eff}}(k) \equiv -2 \frac{d \ln D_S}{d \ln k} \tag{1.4}$$

with $z_{\text{eff}} > 0$. The maximum value of z_{eff}, which we denote by z_Q, occurs at the point of inflexion, or quasiscaling point, as indicated by the large solid circle labeled Q in Fig. 2. Because of the vanishing curvature, there is an interval about Q, the quasiscaling region, within which D_S is well approximated by the quasiscaling behavior $k^{-(1+z_Q)/2}$. It is the existence of the quasiscaling region with $z_Q > 0$ that for many years caused considerable confusion and seemed to indicate a failure of dynamic scaling.

Having accepted the existence of the quasiscaling point, the reader may nevertheless object that the actual determination of the value of z_Q is left wide open and uncontrolled. Granted that the scaling line for D_S lies high, what keeps $D_S(k)$ from plunging arbitrarily steeply down to its lower precritical curve? The answer is that this "plunge," or at least its beginning, is described by a *slow* transient with an exponent w_S linearly proportional to w^* (according to Ref. 4). Thus as $w^* \to 0$ the scaling line moves higher up in Fig. 2 but at the same time the "plunge" becomes slower. The effects tend to compensate and yield a finite limiting value of $z_Q \simeq 0.2$ for $w^* = 0$, as reported in Ref. 1 and as will be established in Sec. V below.

In Secs. II and III we first lay the mode-coupling ground work for the calculation which follows in Secs. IV and V. As will become evident in Sec. V, and in the discussion and summary of Sec. VI, the value of z_Q is relatively insensitive to the mode of calculation, provided that the "boundary conditions" of background and precritical rise are respected. We believe that it is this stability of the phenomenology that lends validity to the differential renormalization-group calculations,[6-8] whose fits to the experimental data might otherwise have to be regarded as fortuitous because of the two-loop limitation.

The reader who is not interested in the details of the ground work in Secs. II and III may wish to skip immediately to the central issue in Sec. IV. For this purpose we collect here the necessary results from Secs. II and III. The object is, of course, to calculate the two functions $D_{S,\psi}(k)$. But to a good approximation we claim that we know *a priori* that the product of the two functions satisfies

$$D_\psi(k) D_S(k) \propto \frac{1}{x} , \tag{1.5}$$

where the proportionality constant is known and where

$$x = \frac{k}{k_c + k} . \tag{1.6}$$

k_c is a certain characteristic value of k. In the asymptotic scaling region (if the latter exists), $x=0$, while in the opposite limit of large noncritical values of k, $x=1$. Because

of Eq. (1.5) it remains only to compute the ratio

$$w(x)\equiv\frac{D_\psi(k)}{D_S(k)}\ , \tag{1.7}$$

which generalizes Eq. (1.3) outside the scaling region. The function $w(x)$ is determined by the "flow" equation

$$\frac{d\ln w}{d\ln x}=W(x,w)\ . \tag{1.8}$$

The solution of Eq. (1.8) connects smoothly the scaling limit $w(0)=w^*\simeq 0$ with the background value $w_B\simeq\frac{1}{2}$. It thus provides an alternative to the interpolation used in Ref. 1. On the basis of various arguments we arrive in Secs. II and III at the linearized expression

$$W=u(x)+v(x)w\ , \tag{1.9}$$

where the end-point constraints are

$$u(0)=-w^*\ , \tag{1.10}$$

$$v(0)=1\ , \tag{1.11}$$

and

$$u(1)+v(1)w_B=-w^*\ . \tag{1.12}$$

The general solution by quadrature of Eqs. (1.8) and (1.9) is presented in Sec. IV. Thus the linearization in w and the restriction to w as the only flow variable enable us to determine the crossover behavior of $D_{S,\psi}$ without resorting to an elaborate computer project, which would tend to obfuscate the essential features of the problem. The solution that we thereby obtain is used in Sec. V in our study of the quasiscaling behavior.

II. MODE COUPLING

In this section we use the mode-coupling formalism of Ref. 4 to arrive at a phenomenological framework for describing the variation of $D_{S,\psi}(k)$ away from their background values $B_{S,\psi}$. We begin in Sec. II A with the precritical rise and return to this important matter with additional details in Sec. III below. This section also deals with (II B) some regularities that can be inferred by varying the order-parameter dimensionality (II C) a resume of the essential features of the scaling solution, and (II D) a differential-flow scheme for studying the onset of scaling.

A. Onset of criticality

We begin with the precritical rise for $D_S(k)$, which is described by the single-loop equation

$$D_S(k)=\frac{g^2}{k^2}\frac{1}{8\pi^3}\int\frac{d^3p}{p^2p'^2}\frac{(p^2-p'^2)^2}{p^2D_\psi(p)+p'^2D_\psi(p')}+B_S\ , \tag{2.1}$$

where g^2 is the usual coupling constant (see Ref. 4). The convolution integration is constrained by conservation of momentum

$$\vec{p}+\vec{p}\,'=\vec{k}\ . \tag{2.2}$$

Equation (2.1) gives the zero-frequency kinetic coefficient. The finite-frequency generalization that we require for self-consistency[4] is achieved by including $k^2D_\psi(k)$ in the denominator of the integrand. Because this is a convergent integral, the range of values of p and p' is set by k. Therefore if $D_\psi(p)$ varies as $p^{-1+\bar{\epsilon}}$ in the vicinity of k, it can be replaced by $D_\psi(k)$ and taken outside the integral. This is permitted if the exponent $\bar{\epsilon}$ is a sufficiently slowly varying function of p. The convolution integral then becomes equal to $k/[2\pi^2D_\psi(k)]$ times

$$I_S(\bar{\epsilon})=\frac{1}{4\pi}\int\frac{d^3p}{p^2p'^2}\frac{(p^2-p'^2)^2}{p^{1+\bar{\epsilon}}+(p')^{1+\bar{\epsilon}}+1}\ , \tag{2.3}$$

where now the intermediate momenta have been scaled to satisfy $\vec{p}+\vec{p}\,'=\vec{1}$. The fractional precritical rise is found by setting $\bar{\epsilon}=1$, substituting Eq. (2.3) into Eq. (2.1), and dividing by the background:

$$\frac{D_S}{B_S}=1+\frac{g^2/2\pi^2}{B_SB_\psi}I_S(1)\frac{1}{k}=1+\frac{k_c}{2k}\ . \tag{2.4}$$

The characteristic wave number is

$$k_c=I_S(1)\frac{g^2/\pi^2}{B_SB_\psi}\ , \tag{2.5}$$

where the integral is found in Appendix A to be $I_S(1)=1.07$.

As discussed in Sec. V below, B_ψ is found from critical ultrasonic attenuation to be of the same order of magnitude as B_S. Substituting $B_\psi\simeq B_S$ into Eq. (2.5) brings this equation, within a numerical factor, into the same form as Eq. (2) of Ref. 1. In Ref. 1 we proceeded to note that Eq. (2.5) yields a value of k_c 2 orders of magnitude smaller than might be expected on the basis of the interatomic spacing, r_s. This results from the smallness of $G\equiv r_sg^2$ relative to B_SB_ψ, i.e., $G\ll B_SB_\psi$. We further attempted to provide some physical understanding of $G\ll B_SB_\psi$ based on the following two effects:

(1) The smallness of the entropy factor in g resulting from the stiffness of the fluid. (This item had to be dropped from Ref. 1 because of space limitations.)

(2) The diverging critical specific heat C_P in the denominator of G. Ahlers, Hohenberg, and Kornblitt[8] have questioned the validity of (2), claiming that k_c is independent of C_P. Of course, $B_S=\lambda_B/C_P$ can be written, where λ_B is the background thermal conductivity, and then to cancel the original factor of C_P^{-1} in G with the C_P^{-1} introduced by B_S into the denominator of Eq. (2.5). But this approach ignores the fact that we already have at hand experimental values for $B_{S,\psi}$, which, so far as we know, have nothing to do with critical dynamics. Therefore, if we want to understand the inequality $G\ll B_SB_\psi$ we should take the right-hand member as given and concentrate our attention on the left-hand member, namely the critical dynamics coupling constant G. An advantage of this point of view was noted in Refs. 2 and 3: The experimental value $(B_SB_\psi)^{1/2}\simeq 1.4\times10^{-4}$ cm^2/sec (see Sec. III B below) is close to the natural limit $D_0=\hbar/m=1.6\times10^{-4}$ cm^2/sec, where $2\pi\hbar$ and m are Planck's constant and the ^{4}He atomic mass, respectively. D_0 is, of course, defined only within a numerical factor of $O(1)$. $2D_0\simeq h/3m$ comes from substituting into the kinetic formula $pl/(3m)$ the unitarity limit $l=\lambda$, where l and $\lambda=h/p$ are the mean free path and the de Broglie wavelength, respectively. As

a consequence, in estimating the size of k_c, we can represent $B_S B_\psi$ in the denominator of Eq. (2.5) by D_0^2. Thus the relative smallness of k_c ensues from the inequality $G \ll \hbar^2/m^2$. Items (1) and (2) above remain as valid sources of this strong inequality, in spite of the criticism of Ahlers, Hohenberg, and Kornblitt.[8] The point of our discussion was intended to be the answer [provided in (1) and (2) above] to the question, "With the background determined from known non-critical dynamics data, how does one understand the relative smallness of G?"

The characteristic wave number as expressed by Eq. (2.5) depends only upon the geometric mean of the background kinetic coefficients and is independent of their ratio. *It is a fortiori and by definition totally insensitive to* w^*. Nevertheless, Ahlers, Hohenberg, and Kornblitt[8] make a point of claiming that in Ref. 1 we assert otherwise; they may have misunderstood our use of the term "critical region" which came one paragraph later, after our equation for k_c. In accord with conventional usage, we were referring in this way to the true asymptotic scaling region, which we observed would shrink because of $w^* \ll 1$. By misidentifying the size of the critical region with k_c, Ahlers, Hohenberg, and Kornblitt[8] evidently arrived at the idea that we were contradicting our own formula for k_c. Let us therefore state quite unequivocally that k_c is independent of w^*.

We refute, in passing, a further criticism by Ahlers, Hohenberg, and Kornblitt[8] of the mode-coupling formalism that we use for our calculations. This is derived in Ref. 4 from the equations of motion, in which we allow for a critical specific heat while keeping the order-parameter time dependence purely relaxational. Although this scheme corresponds to neither their model "E" nor model "F", we reject the assertion that it is not mathematically self-consistent. The self-consistency condition is expressed by Eq. (8) of Ref. 4. In any case, the big difference in results found by Ahlers, Hohenberg, and Kornblitt[8] between models E and F has been shown by Dohm and Volk[7] to be erroneous and to be a consequence of the omission by Ahlers, Hohenberg, and Kornblitt[8] of some terms from their model-F computation. For our present purpose of calculating z_Q we can ignore the critical variation of the specific heat.

B. Natural boundary

As discussed at some length in Ref. 4, some general conclusions concerning the behavior of $D_{S,\psi}(k)$ can be derived from the Sasvari-Schwabl-Szepfalusy[11] (SSS) model. This is a natural generalization of the two-component (i.e., complex) order parameter to an n-dimensional isotropic space with $n(n-1)/2$ generators working in the order-parameter space. For any given component of the order parameter there are $n-1$ generators that can rotate it and bring about its relaxation. There is consequently a natural boundary at $n=1$ in the n-d plane, as shown by the horizontal dashed line in Fig. 3. At this boundary $n-1=0$, and there are no generators to perturb the order parameter. Therefore the order-parameter diffusion coefficient stays at its constant background value

$$D_\psi(k) = B_\psi \tag{2.6}$$

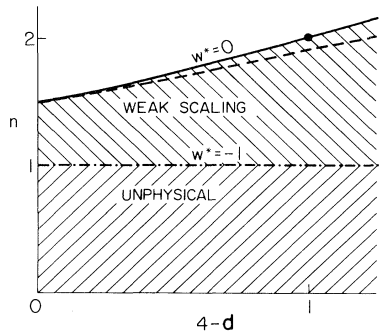

FIG. 3. Parameter boundaries in the n-component SSS (Ref. 11) model for d-dimensional space. The λ transition in liquid helium is represented by $d=3$, $n=2$ (solid circle). w^* is the fixed point value of w, the kinetic coefficient ratio. $w^*=0$ is the dynamic scaling stability boundary, below which dynamic scaling breaks down and is replaced by weak scaling. The dashed line is the two-term ϵ-expansion stability boundary while the solid curve is drawn to include higher terms. The dotted-dashed horizontal line shows the $n=1$ natural boundary for the SSS model.

for all k and to all loop orders. Similarly the entropy diffusion coefficient is given (accurate to all loop orders) by the single-loop expression of Eqs. (2.1) and (2.4). It is convenient to choose units of time and space so that

$$B_S B_\psi = 1 \tag{2.7a}$$

and

$$k_c = \frac{2}{n}\ , \tag{2.7b}$$

which puts Eq. (2.4) into the form

$$\frac{D_S}{B_S} = x^{-1} \tag{2.8a}$$

with Eq. (1.6) generalized by

$$x^{-1} = 1 + \frac{nk_c}{2k} = 1 + \frac{1}{k}\ . \tag{2.8b}$$

It follows that in this limiting case the quasiscaling point has receded to $x=k=0$ and that the quasiscaling exponent is

$$z_Q = 1\ . \tag{2.9}$$

By virtue of Eqs. (2.6), (2.7a), and (2.8a) the product function takes on the simple form

$$s = D_S D_\psi = D_S B_\psi = x^{-1}\ . \tag{2.10}$$

In the next section (II C) we argue that Eq. (2.10), trivially valid in the limit $n \to 1$, is also approximately true independently of n. We expect Eq. (2.10) to be a good approximation in the entire "weak scaling" region of the n-d plane of Fig. 3. This is the region above the natural boundary and below the scaling instability boundary labeled by $w^*=0$. Being unphysical, the region in Fig. 3 below the natural boundary does not provide any useful information. For $n<1$ the SSS model would yield negative values for D_ψ.

The n independence of Eq. (2.10) is important. By fixing the behavior of the product variable *a priori*, it reduces the problem to that of determining only one dependent variable, the ratio $w(x)$. This function will, of course, be n dependent. At the natural boundary Eq. (2.10) yields the linear behavior

$$w=\frac{D_\psi}{D_S}=w_B x \ . \tag{2.11}$$

Equation (2.11) can be described in terms of a "flow," with a constant "flow rate"

$$\frac{d\ln w}{d\ln x}=W=1 \ . \tag{2.12}$$

C. Scaling region

We now return to the physical case $n=2$. It is convenient to measure $D_{S,\psi}$ in units of $(B_S B_\psi)^{1/2}$, which is equivalent to normalizing the background according to Eq. (2.7a). The normalization of Eq. (2.7b) means that we are measuring k in units of $nk_c/2=k_c$. This is equivalent to setting the coupling constant equal to the dimensionless quantity

$$g^2=\frac{\pi^2}{I_S(1)} \ . \tag{2.13}$$

Having normalized the problem in the background and precritical regions, we now skip over the intervening crossover and quasiscaling regions into the asymptotic scaling region, which for the present purposes we assume to exist. In other words, we assume $w^*>0$. The end result is, however, independent of this assumption. Equation (2.1) then reads

$$D_S(k)=\frac{g^2/2\pi^2}{D_\psi(k)}I_S(\tfrac{1}{2})\frac{1}{k}=\frac{k^{-1}}{D_\psi(k)}\frac{\frac{1}{2}I_S(\frac{1}{2})}{I_S(1)} \ . \tag{2.14}$$

[As explained at the end of Sec. 5.2 of Ref. 4 the background term in Eq. (2.1) is cancelled by a high-momentum correction to the integral.] Thus the scaling strength is determined, to single-loop order, by

$$a^2\equiv a_S a_\psi\equiv\lim_{k\to 0}kD_S D_\psi=\frac{\frac{1}{2}I_S(\frac{1}{2})}{I_S(1)} \ . \tag{2.15}$$

Ignoring for the moment the finite-frequency effect, we can get a rough evaluation of Eq. (2.15) from the two-term $\bar{\epsilon}$ expansion[4,14]

$$\bar{I}_S(\bar{\epsilon})=\frac{2}{3\bar{\epsilon}}+\frac{8}{9} \ . \tag{2.16}$$

This gives 1% accuracy for the integrals, as for example $\bar{I}_S(1)=1.55$ (the exact value being $\pi/2=1.57$). Thus

$$a^2\simeq=\frac{\frac{2}{3}+\frac{4}{9}}{\frac{2}{3}+\frac{8}{9}}=\frac{5}{7}=0.71 \ , \tag{2.17}$$

which is brought down to 0.64 by the finite-frequency effect that is evaluated in Appendix A. Estimates of the two-loop vertex correction considerably increase a^2 and bring it somewhat above 1. Because of this numerical result, the product of the kinetic coefficients is expressed approximately by the simple formula

$$D_S D_\psi\equiv s=\frac{1}{k}+O(1) \ , \tag{2.18}$$

valid in the $k\ll 1$ scaling region, where the term of $O(1)$ is negligibly small by comparison with the scaling term k^{-1}. Thus in the scaling region as well as in the background and precritical regions, where $k\simeq 1$, the coefficient of k^{-1} is approximately the same. This statement depends upon the fact, established in Sec. III below, that the precritical strength of D_ψ/B_ψ is nearly equal to that of D_S/B_S and is therefore also given by Eq. (2.4).

The inclusion of the $O(1)$ term in Eq. (2.18) is dictated by the theory of transients developed in Sec. 5.2 of Ref. 4. The product function is expected to deviate from its scaling solution according to

$$s=a^2k^{-1}(1+b_f k^{\omega_f}) \ , \tag{2.19}$$

where the slow transient is absent, to lowest order in ϵ, and the fast-transient exponent is estimated from the ϵ expansion as $\omega_f\simeq 1$. Substitution of this exponent and Eq. (2.17) into Eq. (2.19) gives

$$s=k^{-1}(1+b_f k)=k^{-1}+b_f \ . \tag{2.20}$$

This identifies the $O(1)$ term in Eq. (2.18) with b_f. b_f is a free parameter which remains at our disposal. As in Ref. 1 we choose the transient amplitude so as to have a smooth interpolation formula which bridges between the scaling and precritical regions. Because of Eq. (2.4), which is shown in Sec. III below also to hold for D_ψ/B_ψ, the choice

$$b_f=1 \tag{2.21}$$

is compelling. This is because of the almost exact agreement of the coefficient of k^{-1} for the two extreme regions. We therefore arrive at the interpolation formula

$$s=x^{-1} \tag{2.22}$$

for the entire range $0<x\leq 1$. x is defined, as always, by Eq. (2.8b), so that Eq. (2.22) covers all of the wave-number space, $0<k<\infty$.

The fact that Eq. (2.20) is identical in form to Eq. (2.10) is the basis for the claim of lack of dependence upon n. Such an n independence is not surprising because the pronounced effects of the variation of n are associated with the scaling fixed point value w^*.

The curve in Fig. 3 shows the stability boundary, below which (shaded region) dynamic scaling breaks down and is replaced by "weak" scaling. In the weak-scaling region D_ψ and D_S scale differently. The straight-line version of the stability boundary (dashed line in Fig. 3) has been calculated by DeDominicis and Peliti,[13] by Dohm and Ferrell,[14] and by the present authors in Sec. 4 of Ref. 4. These were two-loop calculations in the ϵ expansion. From the concept of velocity persistence[2,3] it seems that the higher-loop contributions can be approximately represented by the stability boundary shown as the solid curve in Fig. 3, passing exactly through the physical point (solid circle in Fig. 3). Most of the rest of our work will be restricted to this case, i.e., $w^*=0$. We are presently en-

gaged in a three-loop calculation[15] to test the accuracy of the hypothesis of $w^*=0$.

D. Onset of scaling

In this section we derive from the mode-coupling theory a procedure for studying the variation of w from its background value w_B down to its fixed point value $w^*\simeq 0$. Although this information is already contained in the mode-coupling integrals and lends itself to a Padé-type interpolation as in Ref. 1, a convenient alternative approach is to replace the "soft" cutoff on the convolution integral of Eq. (2.1) by an equivalent "hard" cutoff at $p=Ck$ on the simpler integral obtained by using the high-momentum approximation $\vec{p}\approx\vec{p}\,'$. Thus Eq. (2.1) becomes

$$D_S(k)=\frac{1}{3I_S(1)}\int_{Ck}^{\infty}\frac{dp}{p^2D_\psi(p)}+B_S\ , \tag{2.23}$$

upon substituting from Eq. (2.13). The cutoff factor C depends upon the behavior of $D_\psi(p)\propto p^{-1+\bar{\epsilon}}$ in the vicinity of $p=k$. Requiring that Eq. (2.23) be equivalent to Eqs. (2.1) and (2.3) as far as their low-momentum properties are concerned imposes the constraint

$$C^{-\bar{\epsilon}}=\tfrac{3}{2}\bar{\epsilon}I_S(\bar{\epsilon})\ . \tag{2.24}$$

We can eliminate the background term and the high-momentum correction to the integral by differentiating Eq. (2.23) to obtain

$$\begin{aligned}D_S'(k)&=-\frac{1}{k^2D_\psi(k)}\frac{C^{-\bar{\epsilon}}}{3I_S(1)}\left[1+\frac{d\ln C}{d\ln k}\right]\\&=-\frac{1}{2k^2D_\psi(k)}U_S\ ,\end{aligned} \tag{2.25}$$

where, by substitution of Eq. (2.24),

$$U_S=\frac{\bar{\epsilon}I_S(\bar{\epsilon})}{I_S(1)}\left[1+\frac{d\ln C}{d\ln k}\right]\ . \tag{2.26}$$

Here we have neglected $d\bar{\epsilon}/dk$. The above conversion of the mode-coupling integral equation into a "flow"-type differential equation is similar to the equivalence noted by Kawasaki and Gunton[16] between mode coupling and the dynamic renormalization group at single-loop order.

The mode-coupling equation for $D_\psi(k)$ can be treated similarly to yield

$$D_\psi'(k)=-\frac{1}{2k^2D_S(k)}U_\psi\ , \tag{2.27}$$

with the specification of U_ψ to be attended to directly. By multiplying Eq. (2.25) by D_ψ and Eq. (2.27) by D_S we obtain for the product $s=D_SD_\psi$

$$\frac{ds}{dk}=-\frac{1}{2k^2}(U_S+U_\psi)\ . \tag{2.28}$$

The ratio is similarly determined by

$$\begin{aligned}\frac{dw}{dk}&=\frac{1}{2k^2D_S^2}(U_S-U_\psi)\\&=\frac{w}{2k^2s}(U_S-U_\psi)=\frac{2w}{2k(1+k)}(U_S-U_\psi)\ ,\end{aligned} \tag{2.29}$$

where we have substituted Eq. (2.10). Because of $w^*\simeq 0$, $U_\psi\simeq U_S\simeq 1$ at the fixed point, provided the two-loop contributions are included, as discussed above. Thus, in the scaling region,

$$\tfrac{1}{2}(U_S+U_\psi)\simeq U_S\simeq 1\ . \tag{2.30}$$

Taking this to be true for the entire range $0=k\le\infty$ permits us to integrate Eq. (2.28) and recover Eq. (2.10).

The introduction of $x=k/(1+k)$ puts Eq. (2.29) into the simpler form

$$\frac{d\ln w}{d\ln x}=W(w,x)\ , \tag{2.31}$$

where

$$W(w,x)=\tfrac{1}{2}U_S-\tfrac{1}{2}U_\psi \tag{2.32}$$

is considered, in principle, to include all higher-loop contributions. An important property of the "flow" function W is its nodal line $w=w_0(x)$, defined by

$$W(w_0(x),x)=0\ . \tag{2.33}$$

If we assume that the deviation of the actual trajectory $w(x)$ from the nodal line is moderate, the values taken on by W will be relatively small. This serves to justify the linearization, using the nodal line as reference,

$$W(w,x)\simeq[w-w_0(x)]W'=-u(x)+v(x)w\ , \tag{2.34}$$

where

$$v(x)=W'\equiv\left.\frac{\partial W(w,x)}{\partial w}\right|_{w=w_0(x)} \tag{2.35}$$

and

$$u(x)=w_0(x)v(x)\ . \tag{2.36}$$

[A nonlinear modification of Eq. (2.34) is discussed in Secs. IV B and V B below.] By definition, the fixed-point value is

$$w_0(0)=w^*\ , \tag{2.37}$$

while the behavior near the fixed point is controlled by $v(0)$. The slow-transient exponent is known from Sec. 5.2 of Ref. 4 to be $\simeq w^*$, from which it follows

$$v(0)=1\ , \tag{2.38}$$

and by Eq. (2.36)

$$u(0)=w^*\ . \tag{2.39}$$

If we apply the general framework of Eq. (2.34) in the special case of $n=1$ we find, according to Eq. (2.12),

$$W(w,x)=1\ , \tag{2.40}$$

all along the actual trajectory. It follows for $n=1$ from Eqs. (2.34) and (2.39) that $w^*=-1$, which is how the natural boundary is labeled in Fig. 3.

As discussed in the next section, the flow in the precritical region in the vicinity of $x=1$ provides important boundary conditions for Eq. (2.31). We denote the end point of the nodal line by

$$w_1=w_0(1) \tag{2.41}$$

and the corresponding partial derivative by

$$1-c\equiv v(1)=W'|_{x=1} . \tag{2.42}$$

The linear interpolation between Eqs. (2.38) and (2.42) is

$$v(x)=1-cx , \tag{2.43}$$

while the corresponding extension of Eq. (2.39) is

$$u(x)=w^*+bx . \tag{2.44}$$

For $d=3$ the loop expansion is in powers of $(ks)^{-1}=x/k=1-x$. Thus a truncation at two-loop order yields expressions linear in x of the form of Eqs. (2.43) and (2.44), provided certain additional simplifications are made.

An additional boundary condition on the flow function at the upper end of the flow is, from Eqs. (2.43) and (2.44),

$$\begin{aligned} W(w_B,1)&=-u(1)+v(1)w_B \\ &=-w^*-b+(1-c)w_B \\ &=-w^*+w_B-(b+cw_b) , \end{aligned} \tag{2.45}$$

which provides a constraint relating the parameters b and c. This constraint, combined with Eq. (2.42), fixes the parameters completely. At the natural boundary $w^*=-1$ and $W(w_B,1)=1$, while for $w^*=0$ we find in Sec. III A $W(w_B,1)=0$, to a good approximation. Both of these cases are described by

$$W(w_B,1)=-w^* , \tag{2.46}$$

which gives a reasonable interpolation for the intermediate range $-1\le w^*\le 0$. It follows from substitution of Eq. (2.46) into Eq. (2.45) that the parameter constraint is

$$b=(1-c)w_B . \tag{2.47}$$

Equations (2.36), (2.43), and (2.44) imply the nodal line

$$w_0(x)=\frac{u(x)}{v(x)}=\frac{w^*}{1-cx}+b\frac{x}{1-cx} . \tag{2.48}$$

Figure 4 shows two examples of Eq. (2.48) for $w^*=0$ and $w_B=1$, the latter condition requiring $b=1-c$, according to Eq. (2.47). The straight dashed line labeled $W=0$ corresponds to $c=0$ and $b=1$, while the dashed curve is a plot of Eq. (2.48) for $c=\frac{2}{3}$ and $b=\frac{1}{3}$.

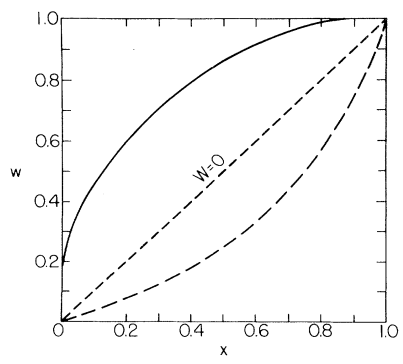

FIG. 4. Nodal lines (dashed) for vanishing flow for two different parameter choices. The nodal line is constrained at the two "anchor" points $x=0$ and $x=1$. The solid curve shows the solution $w(x)$ for the flow equation with the straight nodal line.

III. PRECRITICAL RISE

A. Nonlocal limit

As emphasized in the preceding two sections, the theory of the kinetic coefficients $D_{S,\psi}$ is simplest in the scaling region and in the precritical van Hove region (see Fig. 1). This section is devoted to the latter region. It is particularly important to establish the precritical rise because this is determined entirely by the single-loop integrals and can be calculated rigorously. In this section we continue to work entirely in the nonlocal limit, so as to have only k-dependent functions to deal with. The outcome of the work will be to fix the parameters w_1 and $v(1)$ of Eqs. (2.41) and (2.42). In Sec. III B, which follows immediately below, we turn our attention to the local limit for the purpose of comparing our approach with that of Ahlers, Hohenberg, and Kornblitt.[8]

With the use of units in which k_c, the characteristic wave number of Eq. (2.5), is unity, we have in parallel to Eq. (2.4)

$$\frac{D_\psi}{B_\psi}=1+\frac{U_\psi}{2k} , \tag{3.1}$$

where the coefficient of $1/2k$ is the ratio of two integrals

$$U_\psi=\frac{I_\psi(1,w,w)}{I_S(1)} . \tag{3.2}$$

The denominator is the single-loop entropy integral, for which in Appendix A we find

$$I_S(1)=1.07 . \tag{3.3}$$

The numerator of Eq. (3.2) is the single-loop order-parameter integral

$$I_\psi(\bar\epsilon,w,z)=\frac{1}{4\pi}\int\frac{d^3p/p^2}{(p')^{1+\bar\epsilon}+wp^{1+\bar\epsilon}+z} , \tag{3.4}$$

evaluated in the precritical region, where $\bar\epsilon=1$. The finite-frequency effect (see Ref. 4, Sec. 3) is expressed by setting $z=w$. In our earlier studies of the $\bar\epsilon$ expansion we employed[4,14] the convolution integral

$$\bar I_\psi(\bar\epsilon)\equiv\frac{1}{4\pi}\int\frac{d^3p}{p^2(p')^{1+\bar\epsilon}} , \tag{3.5}$$

which provides a convenient starting point for our present calculation of $I_\psi(\bar\epsilon,w,w)$. We first want to obtain an expression for the integral without the frequency effect, namely,

$$I_\psi(1,w,0)=\frac{1}{4\pi}\int\frac{d^3p/p^2}{p'^2+wp^2} . \tag{3.6}$$

We make contact with our earlier work by setting $z=w=0$ to obtain

$$\begin{aligned} I_\psi(1,0,0)&\equiv\bar I_\psi(\bar\epsilon)|_{\bar\epsilon=1}=\bar I_\psi(1) \\ &=\frac{1}{4\pi}\int\frac{d^3p}{p^2p'^2}=\frac{\pi^2}{4} . \end{aligned} \tag{3.7}$$

Our immediate goal is to find the w dependence of $I_\psi(\bar{\epsilon},w,0)$. Throughout this section we keep $\bar{\epsilon}=1$. A simple interchange of p' with p in Eq. (3.6) followed by substitution of Eq. (3.7) yields for the special case $w=1$

$$I_\psi(1,1,0)=\frac{1}{4\pi}\int\frac{d^3p/p^2}{p^2+p'^2}=\frac{1}{4\pi}\int\frac{d^3p'/p'^2}{p^2+p'^2}$$
$$=\frac{1}{8\pi}\int\frac{d^3p}{p^2+p'^2}\left[\frac{1}{p^2}+\frac{1}{p'^2}\right]=\tfrac{1}{2}I_\psi(1)=\frac{\pi^2}{8}\ . \tag{3.8}$$

Comparing Eqs. (3.8) and (3.7) we see that $I_\psi(1,w,0)$ drops by a factor of 2 when w goes from 0 to 1. The initial drop is given by the subtraction integral

$$I_\psi(1,w,0)-I_\psi(1,0,0)$$
$$=\frac{-w}{4\pi}\int\frac{d^3p'/p'^2}{p'^2+wp^2}\simeq\frac{-w}{4\pi}\int\frac{d^3p'/p'^2}{p'^2+w}$$
$$=-w\int_0^\infty\frac{dp'}{p'^2+w}=-\frac{\pi}{2}\sqrt{w}\ , \tag{3.9}$$

valid for $0\le w\ll 1$. The approximation $p=|\vec{k}-\vec{p}\,'|\simeq k=1$ is justified by the fact that most of the strength of the integral is concentrated in the region $p'\ll 1$. Substituting Eqs. (3.7) and (3.9) into Eq. (3.6) gives

$$I_\psi(1,w,0)\simeq\frac{\pi^2}{4}-\frac{\pi}{2}\sqrt{w}\ , \tag{3.10}$$

for $0\le w\ll 1$. We extend Eq. (3.10) to the entire interval $0\le w\le 1$ by means of the Padé-type approximant

$$I_\psi(1,w,0)=\frac{\pi^2}{4}-\frac{\pi}{2}\left[\frac{w}{1+\beta w}\right]^{1/2}\ , \tag{3.11}$$

where imposing Eq. (3.8) requires

$$\beta=\frac{16}{\pi^2}-1=0.621\ . \tag{3.12}$$

A check on the accuracy of Eq. (3.11) is provided by the derivative of Eq. (3.6) at $w=1$, for which an analytic integration readily yields ($\partial/\partial w$ being indicated by a prime)

$$I'_\psi(1,1,0)=-\frac{1}{4\pi}\int\frac{d^3p}{(p^2+p'^2)^2}$$
$$=-\frac{\pi}{8}=-\frac{1}{\pi}I(1,1,0)\ . \tag{3.13}$$

Differentiation of Eq. (3.11) gives

$$I'_\psi(1,1,0)=-\frac{1}{2(1+\beta)}I(1,1,0)$$
$$=-\frac{1}{3.24}I(1,1,0)\ , \tag{3.14}$$

smaller than the exact value of Eq. (3.13) by 3%. We are thus assured that Eq. (3.11), plotted as the upper curve in Fig. 5, is a faithful representation of $I_\psi(1,w,0)$ vs w to within an accuracy of the order of 1% over the entire interval $0\le w\le 1$. Because we do not need Eq. (3.11) for $w>1$ the fact that it becomes a poor approximation in this range is of no consequence. (Instead of vanishing when $w\to\infty$, it has the finite limiting value of 0.30.)

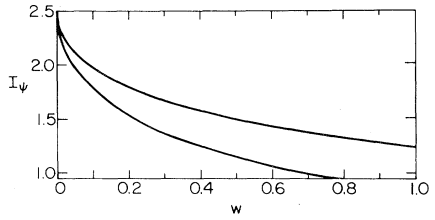

FIG. 5. Precritical single-loop order-parameter integral vs w. The upper curve shows $I_\psi(1,w,0)$ and drops by a factor of 2 at $w=1$. The lower curve, for $I_\psi(1,w,w)$, includes the frequency effect and drops by a factor of 3.

We now include the frequency effect by setting $z=w$ in Eq. (3.4) to obtain

$$I_\psi(1,w,w)=\frac{1}{4\pi}\int\frac{d^3p/p^2}{p'^2+wp^2+w}\ . \tag{3.15}$$

Again we will use a Padé-type approximant, with the initial drop still of the form of Eq. (3.10), except with $2w$ appearing in place of 2. Thus instead of Eq. (3.11) we have

$$I_\psi(1,w,w)\simeq\frac{\pi^2}{4}-\frac{\pi}{2}\left[\frac{w}{1+\beta' w}\right]^{1/2}\ , \tag{3.16}$$

with β' to be fixed by $I_\psi(1,w,w)$, evaluated at $w=1$. As before, we exchange p' for p, which produces now the simplification

$$I_\psi(1,1,1)=\frac{1}{8\pi}\int\frac{d^3p}{1+p^2+p'^2}\left[\frac{1}{p^2}+\frac{1}{p'^2}\right]$$
$$=\tfrac{1}{2}\bar{I}_\psi(1)\left[1-\left\langle\frac{1}{1+p^2+p'^2}\right\rangle\right]\ , \tag{3.17}$$

where the angular brackets denote the weighted average

$$\langle A\rangle\equiv\frac{1}{\bar{I}_\psi(1)}\frac{1}{4\pi}\int\frac{d^3p}{p^2p'^2}A\ . \tag{3.18}$$

Numerical integration indicates that the effective average value for p^2 and p'^2 is 1.00 (to 1% accuracy), so that the required average is

$$\left\langle\frac{1}{1+p^2+p'^2}\right\rangle=\frac{1}{3}\ . \tag{3.19}$$

Substituted into Eq. (3.17), this yields

$$I_\psi(1,1,1)=\tfrac{1}{3}\bar{I}_\psi(1)=\frac{\pi^2}{12}\ , \tag{3.20}$$

a drop by a factor of 3 instead of by the factor of 2 found in Eq. (3.8). Imposing this factor of 3 drop on Eq. (3.16) gives

$$\beta'=\frac{18}{\pi^2}-1=0.824\ . \tag{3.21}$$

The plot of Eq. (3.16) versus w is shown as the lower curve in Fig. 5. The marked effect of the finite frequency is evident from a comparison of the two curves.

Our goal here has been to determine the boundary conditions on the "flow" function W in the background limit $k\to\infty$. w_1, the intercept of the nodal line, is determined

from Eq. (2.32) by

$$W(w_1,1)=\tfrac{1}{2}U_s-\tfrac{1}{2}U_\psi=\tfrac{1}{2}(1-U_\psi)=0\ , \tag{3.22}$$

or $U_\psi=1$. By Eq. (3.2) this requires $I_\psi(1,w_1,w_1)=I_s(1)=1.07$. [The substitution of $U_S=1$ follows from setting $\bar{\epsilon}=1$ in Eq. (2.26).] From Eqs. (3.16) and (3.21) this condition is satisfied for

$$w_1=0.59\ , \tag{3.23}$$

as is also apparent from the lower curve of Fig. 5. The derivative at this value of w gives

$$v(1)=W'|_{x=1,\ w=w_1}=-\left.\frac{dU_\psi}{dw}\right|_{w=w_1}=0.37\ . \tag{3.24}$$

As will be established in Sec. V A below, the actual background value at $x=1$ is $w_B=0.5$. Thus the strength of the flow function in the background and precritical region, from Eqs. (2.32), (3.2), (3.16), and (3.21) is

$$W_B\equiv W(w_B,1)=\frac{1}{2}-\frac{1}{2I_S(1)}I_\psi(1,\tfrac{1}{2},\tfrac{1}{2})=-0.03\ , \tag{3.25}$$

consistent with Eqs. (3.23) and (3.24). As $|W_B|$ is an order of magnitude smaller than the typical value of W in the crossover region, we will neglect it. Thus

$$W_B=0\ , \tag{3.26}$$

the boundary condition of vanishing background flow.

B. Local limit

All of our work is carried out at the λ point in the nonlocal limit, where we have to deal only with functions of the single variable k. This makes it difficult to compare in detail our results with those of Dohm and Folk[7] and of Ahlers, Hohenberg, and Kornblitt.[8] By working away from the λ point these authors have the more complicated problem of determining functions not only of the wave number k but also of the inverse correlation length κ. This approach to the problem seems to us inadvisable at the present time because accurate three-dimensional scaling functions for the k-κ plane are not available. This manner of treating the problem is,however, feasible in the precritical van Hove region where the single-loop integrals simplify the problem considerably. In this region we shall exhibit some discrepancies which seem to indicate errors or inaccuracies in the work of the above authors.

The essential simplification in the precritical region is that the kinetic coefficients $D_{S,\psi}$ that occur in the denominators of the single-loop integrals can be approximated by their background values $B_{S,\psi}$. It follows that to this accuracy the required scaling functions, which are in general quite complicated, reduce to $B_S p^2$ and $B_\psi(p^2+\kappa^2)$ for $\gamma_{S,\psi}(p,\kappa)$, the entropy and order-parameter decay rates, respectively. In the local limit the external momentum k vanishes so that according to Eq. (2.2) the internal momenta are of equal magnitude

$$p'=|\vec{p}\,'|=|-\vec{p}\,|=p\ . \tag{3.27}$$

Scaling p now in units of κ rather than k, the single-loop entropy integral becomes in the local limit and at zero frequency

$$I_S^L(1)=\frac{2}{3}\frac{1}{4\pi}\int\frac{p^2d^3p}{(p^2+1)^3}=\tfrac{2}{3}\int_0^\infty\frac{p^4dp}{(p^2+1)^3}=\frac{\pi}{8}\ , \tag{3.28}$$

down by a factor of 4 from its zero-frequency nonlocal value of $\bar{I}_S(1)=\pi/2$. By contrast, the order-parameter single-loop integral does not change as much. Its zero-frequency local expression is

$$I_\psi^L(1,w)=\frac{1}{4\pi}\int\frac{d^3p/(p^2+1)}{p^2+w(p^2+1)}=\frac{\pi}{2}\left[1-\left[\frac{w}{1+w}\right]^{1/2}\right], \tag{3.29}$$

down by roughly a factor of 2 from $I_\psi=(1,w,0)$ of Eq. (3.11), in the vicinity of $w=\frac{1}{2}$. From Eqs. (3.28) and (3.29) the "flow," $dw/d\kappa$, in terms of the variable κ rather than k, is proportional to

$$I_S^L(1)-I_\psi^L(1,w)\propto\left[\frac{w}{1+w}\right]^{1/2}-\frac{3}{4}\ , \tag{3.30}$$

the zero of which gives the nodal line intercept at

$$w_{1L}=\tfrac{9}{7}\simeq 1.29\ . \tag{3.31}$$

Comparing this with what we found in Eq. (3.23) in the nonlocal limit, we have

$$w_{1L}/w_1\simeq 2.2\ , \tag{3.32}$$

a consequence of the marked disparity that we noted above between the behaviors of the scaling functions for the entropy and order-parameter single-loop integrals.

Equations (3.32) and (3.31) illustrate the advantage of working in the nonlocal limit. Because of Eq. (3.26), dw/dk is positive definite and *the flow of w with respect to k is monotonic.* On the other hand, Eq. (3.30) requires $dw/d\kappa<0$ as $\kappa\to\infty$, so that *the flow with respect to κ is nonmonotonic.* Thus $w(\kappa)$ vs κ *must have a maximum* at intermediate values of κ, which makes an accurate interpolation through the problematic crossover region more difficult to achieve.

Equations (3.30) and (3.31) are *rigorous* results, which unfortunately are not to be found in the work of Dohm and Folk[6,7] or Ahlers, Hohenberg, and Kornblitt.[8] The w dependence written down by these authors is not of the form of Eq. (3.30), being instead proportional to $1-2/(1+w)$, a single-term ϵ-expansion expression. They have therefore $w_{1L}=1$, in disagreement with Eq. (3.31). This error is evidently the result of a too great reliance by these authors on low-order ϵ-expansion expressions. We totally avoid the ϵ expansion in this paper. Whenever an approximation is required for evaluating the nonlocal convolution integrals we use the more accurate $\bar{\epsilon}$ expansion. But we emphasize again that Eq. (3.30), being evaluated in the local limit, *involves no approximation. It serves as a criterion for the validity of any flow equation in κ.*

IV. CROSSOVER REGION

Our task is to determine the monotonic variation of $w(x)$ between its limiting values of $w(0)=w^*\simeq 0$ (scaling fixed point) and $w(1)=w_B=O(1)$ (background). In the preceding section we have fixed the precritical variation away from background for $x\simeq 1$. In Sec. IV A below we characterize the first variation of $w(x)$ from its fixed point value, for $0<x\ll 1$, by the method of transients. This will prepare us for the general solution in Sec. IV B, which connects the two ends and covers the entire interval $0\le x\le 1$. In Sec. IV C we demonstrate how the solution of the flow equation provides the desired interpolation through the intermediate crossover region. Sec. IV D concludes with a sketch of a first-order correction that makes it possible to improve further the accuracy of our computational scheme.

A. Slow transient

In the vicinity of the scaling fixed point $(x,w)=(0,w^*)$ we can approximate the functions $u(x)$ and $v(x)$ of the flow function W by Eqs. (2.39) and (2.38) to obtain

$$\frac{d\ln w}{d\ln x}=W(x,w)\simeq W(0,w)$$

$$=-u(0)+v(0)w=w-w^* . \tag{4.1}$$

Thus

$$\frac{d(w-w^*)}{d\ln x}=w(w-w^*)$$

$$=w^*(w-w^*)+(w-w^*)^2 . \tag{4.2}$$

If we neglect the quadratic term, this becomes the linearized transient equation

$$\frac{d\ln(w-w^*)}{d\ln x}=w^* , \tag{4.3}$$

the solution of which is

$$w=w^*(1+b_s x^{\omega_s})\simeq\frac{w^*}{1-b_s x^{\omega_s}} , \tag{4.4}$$

where the "slow-transient" exponent is

$$\omega_s=w^* , \tag{4.5}$$

as a consequence of Eq. (2.38). Both forms of Eq. (4.4) are equivalent for a weak transient. The final form is preferred because it correctly takes into account the quadratic term in Eq. (4.2), as noted by Hohenberg *et al.*[5] and as readily verified by substitution into Eq. (4.2). The denominator of Eq. (4.4) comes up into the numerator when calculating $D_S^2=s/w$. In Ref. 1 we emphasized that this *negative slow transient* (negative because $b_s>0$) is the essential qualitative reason that the effective exponent for D_S is greater than the exponent that would be expected from dynamic scaling.

To facilitate the passage to the limit $w^*\to 0$ we write the slow-transient amplitude as

$$b_s=e^{-w^* c_s} . \tag{4.6}$$

In this limit we find

$$w=\frac{1}{c_s+\ln x^{-1}} , \tag{4.7}$$

where c_s is a number of order unity. Equation (4.7) provides the desired characterization of the first variation of w, for $0<x\ll 1$, away from its fixed-point value $w^*=0$. In the spirit of Ref. 1 we could at this stage, by a suitable choice of c_s, fit Eq. (4.7) on to some reasonable interpolating function having the required behavior in the precritical region. We found in Ref. 1 that these restrictions left little freedom in the choice of function. In the present approach, however, any such freedom is removed by explicitly solving the flow equation, as carried out in the next subsection. The solution yields a specific value for c_s. One such case is shown by the solid curve in Fig. 6, where we have plotted w vs $k=x/(1-x)$ for $c_s=-0.43$.

B. General solution

In the crossover region it is difficult to extract the k dependence directly from the mode-coupling integrals. For this reason, in Sec. II D we have transformed these equations into their differential form. Equations (1.5) and (2.10) specify the variable s, so that it is only the crossover behavior of w that remains to be determined. This is found in general from Eqs. (1.8) and (1.9). By the variable change $y=w^{-1}$ these equations assume the form

$$\frac{dy}{dx}=-\frac{1}{wx}\frac{d\ln w}{d\ln x}=-\frac{W}{xw}=\frac{u}{x}y-\frac{v}{x} . \tag{4.8}$$

The general solution is

$$y(x)=-e^{-X(x)}\int^x\frac{dx''}{x''}v(x'')e^{X(x'')} , \tag{4.9}$$

where

$$X(x)=\int_x^1\frac{u(x')}{x'}dx' . \tag{4.10}$$

Imposing the background boundary condition

$$y(1)=w_B^{-1} \tag{4.11}$$

fixes the constant of integration so that Eq. (4.9) becomes

$$w^{-1}=e^{-X(x)}\left[w_B^{-1}+\int_x^1\frac{dx'}{x'}v(x')e^{X(x')}\right] . \tag{4.12}$$

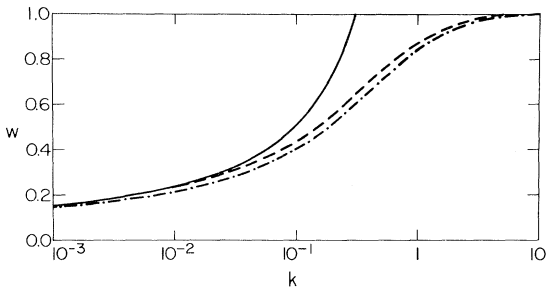

FIG. 6. Kinetic coefficient ratio $w=D_\psi/D_S$ vs wave number for two different parameter choices. The slow transient (solid curve) is an accurate representation for $k\le 0.03$.

Equation (4.12) is the general solution of the flow equation by quadrature. Substitution of Eq. (2.44) gives

$$X=w^*\ln x^{-1}+b(1-x) \tag{4.13}$$

and

$$e^X=x^{-w^*}e^{b(1-x)} . \tag{4.14}$$

Substituting Eqs. (4.14) and (2.44) into Eq. (4.12) we find

$$w^{-1}=x^{w^*}e^{-b(1-x)} \times\left[w_B^{-1}+\int_x^1\frac{dx'}{(x')^{1+w^*}}(1-cx')e^{b(1-x')}\right] . \tag{4.15}$$

The integral in Eq. (4.15) is expressible in terms of the incomplete Γ function. If we restrict our attention to the actual case of interest, $w^*=0$, the incomplete Γ function reduces to the more convenient integral exponential function

$$E_1(x)=-\mathrm{Ei}(-x)=\int_x^\infty\frac{dt}{t}e^{-t} . \tag{4.16}$$

As x is restricted to the interval $0\le x\le 1$, it is convenient to work with the function

$$\bar{E}_1(x)\equiv E_1(x)-E_1(1) . \tag{4.17}$$

In terms of this function the integration in Eq. (4.15) can be written as

$$w^{-1}=-\frac{c}{b}+\left[w_B^{-1}+\frac{c}{b}\right]e^{-b(1-x)} +e^{bx}[\bar{E}_1(bx)-\bar{E}_1(b)] . \tag{4.18}$$

Because of the limited range of the argument, a Taylor's series gives rapid convergence for the function $\bar{E}_1(x)$. For $x\to 0$ we must separate the logarithmic part of the function, obtaining

$$\bar{E}_1(x)=\ln\frac{1}{x}-C_0+x-\frac{x^2}{2\times 2!}+\frac{x^3}{3\times 3!}-\cdots , \tag{4.19}$$

where

$$C_0=1-\frac{1}{2\times 2!}+\frac{1}{3\times 3!}-\cdots\simeq 0.797 . \tag{4.20}$$

For $0<x\ll 1$ all of the terms linear and higher in Eq. (4.18) can be dropped, so that Eq. (4.17) assumes the simpler form of a constant added to $\ln x^{-1}$. Comparing this with Eq. (4.7), we identify the constant as the slow-transient parameter

$$c_s=-\frac{c}{b}+\left[w_B^{-1}+\frac{c}{b}\right]e^{-b}+\ln\frac{1}{b}-C_0-\bar{E}_1(b) . \tag{4.21}$$

To demonstrate the application of the above equations we consider the following convenient choice of parameters: $b=1$, $c=0$, and $w_B=1$. (In Sec. V we reduce w_B and adopt the more realistic background value of $w_B=0.5$.) Thus Eq. (4.21) gives

$$c_s=e^{-1}-C_0=-0.43 , \tag{4.22}$$

the value used in plotting Eq. (4.7) as the solid curve in Fig. 6. The full course of w for this choice of parameters is given by Eq. (4.18) as

$$w=[e^{x-1}+e^x\bar{E}_1(x)]^{-1} , \tag{4.23}$$

which is plotted versus x in Fig. 4 and versus k as the dashed curve in Fig. 6.

An alternative simple choice of parameters is $b=0$ and $c=1$. In this case the integral exponential function disappears from the problem and Eq. (4.18) takes the form

$$w=\frac{1}{c_s+x+\ln x^{-1}} , \tag{4.24}$$

where the slow-transient parameter is

$$c_s=w_B^{-1}-1 , \tag{4.25}$$

and vanishes for $w_B=1$. Equation (4.24) is plotted versus k as the dotted dashed curve in Fig. 6. It is evident that in spite of the difference in parameter choice the two curves for w vs k are close together, nowhere differing by more than 10%. This corresponds to only a 5% effect in $D_{\psi,S}$. The reason for the smallness of the effect is that the difference in the flow rate for these two cases is

$$\Delta W=(1-w)x . \tag{4.26}$$

The flow trajectory is parallel to the axes at its two ends and stays in the upper left half of Fig. 4, thus guaranteeing that one or the other of the factors in ΔW is small. Because of this insensitivity we will use $b=0$ and $c=1$ for the rest of our work. This preference is dictated by the following.

(i) Equations (2.42) and (3.24), which give

$$c=1-0.37=0.63 , \tag{4.27}$$

obviously closer to $c=1$ than to $c=0$.

(ii) The simplicity of Eq. (4.24), which is equivalent to merely adding x to the denominator of Eq. (4.7). This slight but significant change in the slow-transient solution stops it from diverging at $x=\exp(c_s)$ and instead causes w to approach its background value with vanishing slope, as required by Eq. (3.26).

We note in passing that Eqs. (1.8) and (1.9) can be generalized for the separable case $u=0$ to

$$\frac{d\ln w}{d\ln x}=v(x)f(w) , \tag{4.28}$$

where $f(w)$ can be an arbitrary function. The solution by quadrature is

$$\int_w^{w_B}\frac{dw'}{w'f(w')}=\int_x^1\frac{dx'}{x'}v(x') , \tag{4.29}$$

which determines w implicitly as a function of x. An example of a more general flow function is suggested by the lowest-order (i.e., single-term) ϵ expansion, which gives

$$f(w)=(n-1)\frac{w}{1+w} , \tag{4.30}$$

applicable at $\epsilon=0$ on the stability boundary (cf. Fig. 3) where $n=\frac{3}{2}$. Generalization of Eq. (4.30) to $n=2$ and use of $v(x)=1-x$ give

$$W_{\mathrm{NL}}(w,x)=(1-x)\frac{w}{1+w}\ , \tag{4.31}$$

a prototype for a nonlinear generalization of Eq. (2.34). Equation (4.29) then reads explicitly

$$\frac{1}{w}-\frac{1}{w_B}+\ln\frac{w_B}{w}=-1+x+\ln\frac{1}{x}\ . \tag{4.32}$$

C. Interpolating function

Equations (2.22) and (4.24) for the product s and the ratio w, respectively, provide the desired interpolating functions for the separate kinetic coefficients as

$$D_\psi=\sqrt{sw}=(x^2+c_sx+x\ln x^{-1})^{1/2} \tag{4.33}$$

and

$$D_S=\sqrt{s/w}=(1+c_sx^{-1}+x^{-1}\ln x^{-1})^{1/2}\ . \tag{4.34}$$

For the special case ($w_B=1$) of $c_s=0$, Eq. (4.34) becomes

$$D_S=(1+x^{-1}\ln x^{-1})^{1/2}\ , \tag{4.35}$$

which is plotted versus x as the solid curve in Fig. 7. An approximation which is valid in the background and precritical regions is $w\simeq w_B$, so

$$D_S\simeq\frac{w_B^{-1/2}}{\sqrt{x}}=\frac{1}{\sqrt{x}}\ , \tag{4.36}$$

as shown in Fig. 7 by the straight dashed line. This is labeled FAST because Eq. (2.22) for s includes the fast transient. The dashed curve labeled SLOW includes the slow transient in

$$D_S\simeq\frac{1}{\sqrt{x}}(\ln x^{-1}+c_s)^{1/2}=\frac{\ln^{1/2}x^{-1}}{\sqrt{x}}\ , \tag{4.37}$$

which we obtain by substituting Eq. (4.7) into Eq. (4.34). These curves, which are similar to those of Fig. 2 of Ref. 1, show how the full expression for D_S in Eq. (4.35) provides a natural interpolation between the large- and small-x approximations of Eqs. (4.36) and (4.37), respectively. ("Large" x means $0.5\le x\le 1$.)

Equation (4.35) is shown again in Fig. 8. Here it is plotted versus k as the solid curve labeled 0. The corresponding expression

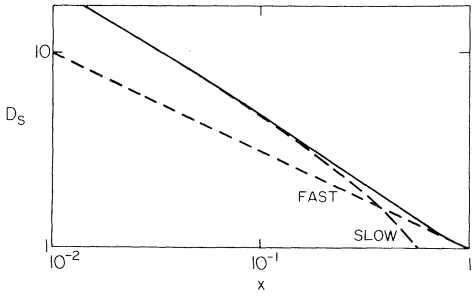

FIG. 7. Entropy diffusion coefficient vs x. The complete variation (solid curve) is an interpolation between the dashed straight line, which contains only the fast transient (and describes correctly the precritical rise), and the dashed curve containing the slow transient. The background ratio was taken as $w_B=1$.

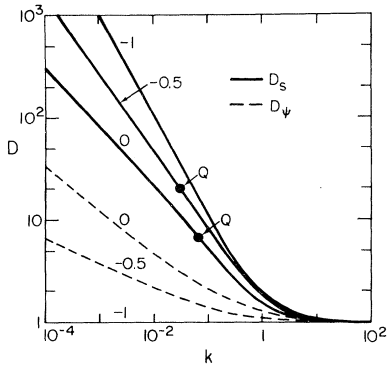

FIG. 8. Kinetic coefficients $D_{S,\psi}$ vs wave number k for $w^*=-1$, 0.5, and 0, the latter being the case of physical interest. The quasiscaling point (solid circle labeled Q) recedes to smaller values of k as w^* becomes more negative. $w^*=-1$ represents the natural boundary of the SSS model. The background ratio was taken as $w_B=1$.

$$D_\psi=(x^2+x\ln x^{-1})^{-1/2} \tag{4.38}$$

is exhibited as the dashed curve labeled 0. The behavior of $D_{\psi,S}$ for $w^*=-1$ (natural boundary) is shown by the constant $D_\psi=1$ at the bottom of Fig. 8 and by the uppermost curve $D_S=x^{-1}$, labeled -1. The intermediate curves labeled -0.5 (dashed for D_ψ and solid for D_S) have been calculated from Eq. (4.15) for $w^*=-0.5$, $w_B=1$, $b=0$, and $c=1$.

D. First-order correction

Our solution for $w(x)$ in the crossover region is based on the flow function W of Eq. (2.34), linearized in w. Because W and w are constrained at the two end points, we expect this treatment not to be sensitive to the exact form of W and to yield the 10% accuracy that we seek. Here, nevertheless, to improve the accuracy further, we set up a simple first-order perturbation calculation of the percentage correction

$$y=\frac{\Delta w}{w} \tag{4.39}$$

produced by ΔW, the deviation of the true value of W from its approximate expression, Eq. (2.34). With

$$\Delta\ln w=\ln(1+y)\simeq y \tag{4.40}$$

we find the first-order change in the flow equation

$$\Delta\frac{d\ln w}{d\ln x}=\frac{dy}{d\ln x}=\Delta W+wW'y\ , \tag{4.41}$$

where W' is defined in Eq. (2.35). Equation (4.41) is of the standard form

$$\frac{dy}{dx}-Py=Q \tag{4.42}$$

with

$$y=e^{\int P\,dx}\int dx\,Qe^{-\int P\,dx}\ , \tag{4.43}$$

where

$$P=\frac{wW'}{x} \tag{4.44}$$

and

$$Q=\frac{\Delta W}{x} . \tag{4.45}$$

The solution is particularly simple for the separable case $u=0$. If we approximate W' by its unperturbed value v, then

$$P=\frac{wW'}{x}=\frac{vw}{x}=\frac{W}{x}=\frac{d\ln w}{dx} \tag{4.46}$$

by Eq. (2.34), which gives

$$e^{\int P\,dx}=w . \tag{4.47}$$

Because $\Delta W\to 0$ as $x\to 0$ the integral in Eq. (4.43) converges. From Eq. (4.47) and $w\to 0$ it then follows that $y\to 0$ as $x\to 0$. The boundary condition $y\to 0$ at the other end, $x\to 1$, is satisfied by an appropriate choice of the constant of integration. Thus the desired first-order correction is

$$\Delta w(x)=-w^2(x)\int_x^1 \frac{dx'}{x'}\frac{\Delta W(x')}{w(x')} , \tag{4.48}$$

with $w(x)$ given by Eq. (4.24).

It is convenient to define by means of Eq. (4.48) an x-dependent first-order change in the slow-transient parameter

$$\Delta c_s(x)\equiv\Delta w^{-1}(x)=\int_x^1 \frac{dx'}{x'}\frac{\Delta W(x')}{w(x')} . \tag{4.49}$$

This combined with Eq. (4.24) enables us to write $\tilde{w}(x)\equiv w(x)+\Delta w(x)$, the first-order corrected solution, as

$$\tilde{w}(x)=\frac{1}{c_s+\Delta c_s(x)+x-\ln x} . \tag{4.50}$$

From Eq. (4.49) we see that the shift in the slow-transient parameter is

$$\Delta c_s(0)=\int_0^1 \frac{dx}{x}\frac{\Delta W(x)}{w(x)}=\int_0^1 \frac{dx}{x}\Delta\frac{W}{w} , \tag{4.51}$$

the final form being valid independently of the $u=0$ assumption. It can also be obtained from the identity

$$c_s=w_B^{-1}-\int_0^1 \frac{dx}{x}\left[1-\frac{W}{w}\right] . \tag{4.52}$$

By comparing the dashed and dotted-dashed curves in Fig. 6 (which correspond to a difference of $\Delta c_s=0.43$), we see that within the tolerance of 10% accuracy for $D_{\psi,S}$ we can neglect the first-order correction provided that it satisfies the criterion

$$|\Delta c_s(0)|<1 . \tag{4.53}$$

Because of the boundary constraints, $W/w=1$ at $x=0$ and drops to zero at $x=1$. The natural scale for the first-order correction is therefore expected to be

$$\left|\frac{\Delta W}{w}\right|<1 , \tag{4.54}$$

which would cause Eq. (4.53) to be satisfied more or less automatically.

If it is desired to take into account Δs, the deviation of s from x^{-1} [the ideal behavior specified by Eq. (2.22)], it is possible to proceed in a manner similar to the above and to calculate the first-order correction from two simultaneous first-order differential equations linear in Δw and Δs.

V. QUASISCALING

The ratio $w=D_\psi/D_S$ is shown in Fig. 4 as a function of x and in Fig. 6 as a function of k. D_S is plotted versus x in Fig. 7, while both kinetic coefficients are shown versus k in Fig. 8. For the sake of simplicity and in order to illustrate as clearly as possible the basic ideas involved, we have carried out all of these computations with the background parameter arbitrarily fixed at $w_B=1$. We now have the task of determining the most realistic and reliable value for w_B, from noncritical background data far from the λ point. We find B_ψ by applying our theory[17] of ultrasonic attenuation to the large body of data that is available for this phenomenon. As we shall soon see, in Sec. V A below, we are led to $w_B=0.5$, the value we proceed to use for the computation of w and hence of $D_{\psi,S}$.

In Sec. V B below we introduce the idea of quasiscaling from a general point of view, and then proceed to calculate the quasiscaling exponent z_Q. For $w_B=0.5$ we find $z_Q=0.18$, which is consistent with our earlier and rougher estimate in Ref. 1. In Sec. V B we also calculate the dependence of z_Q on w^* for $w^*<0$; this result will become applicable if it eventually turns out that, because of the three-loop[15] and higher-loop contributions, the stability boundary in Fig. 3 passes higher and the physical point lies in the weak-scaling region.

A. Background parameters

We now proceed to fix the actual value of $w_B=B_\psi/B_S$ from the separate empirical values for B_ψ and B_S. Ultrasonic attenuation provides the necessary information for B_ψ. The ratio of the attenuation α at the reduced temperature $t=(T-T_\lambda)/T_\lambda\geq 0$ to the λ-point attenuation α_λ is predicted by the theory (for frequencies $\omega/2\pi>1$ MHz) to be

$$\frac{\alpha}{\alpha_\lambda}=\frac{|L|_\lambda^2}{|L|^2}\frac{2}{\pi}\mathrm{Im}L , \tag{5.1a}$$

where $|L|$ is the absolute value of

$$L(\gamma_\psi,\omega)=\ln\frac{2\gamma_c}{(4\gamma_\psi^2+\omega^2)^{1/2}}-\frac{2}{\Omega}\tan^{-1}\left[\frac{\Omega}{2}\right]+B +i\left[\tan^{-1}\left[\frac{\Omega}{2}\right]-\frac{1}{\Omega}\ln\left[1+\frac{\Omega^2}{4}\right]\right] . \tag{5.1b}$$

Thus $\mathrm{Im}L$ is a function only of the reduced frequency

$$\Omega=\frac{\omega}{\gamma_\psi} . \tag{5.2}$$

This definition is a factor of 2 larger than the one that we used before.[17] $|L|_\lambda$ is the λ point ($\Omega\to\infty$) limit of $|L|$, and γ_c and B are certain background parameters for the fluid. The order-parameter relaxation rate

$$\gamma_\psi = B_\psi \kappa^2 = B_\psi \kappa_0^2 t^{2\nu} \tag{5.3}$$

is here in the *local* limit and is a function of κ rather than of k, as in the rest of the paper. Hyperscaling and two-scale factor universality require $\nu=\frac{2}{3}$ and $\kappa_0=0.70$ Å^{-1}. Figure 9 shows a plot of $(2/\pi)\mathrm{Im}L$ from Eq. (5.1b) versus Ω. The characteristic crossover frequency at which ImL equals the value half that at $\Omega=\infty$ is

$$\Omega_{1/2}=4.7 . \tag{5.4}$$

The points in Fig. 9 show the experimental data of Tozaki and Ikushima.[18] In plotting these points we have chosen

$$B_\psi = 1.0\times 10^{-4} , \tag{5.5}$$

in units of cm^2/sec, so as to bring the temperature scale of the measurements into agreement with Eqs. (5.1a) and (5.1b). As is evident in Fig. 9, the resulting fit of the theoretical scaling curve to the data is excellent. [In order to achieve this improved fit we have chosen the B_ψ in Eq. (5.5) to be 20% smaller than the value that we used previously.]

The entropy coefficient in the local limit is the familiar thermal-diffusion coefficient

$$D_S = \frac{\lambda}{C_P} , \tag{5.6}$$

which acquires temperature dependence both from the thermal conductivity in the numerator and the specific heat at constant pressure in the denominator. The temperature dependence of the latter has been reviewed by us recently.[19] Because C_P decreases away from the λ point, D_S exhibits a minimum, close to the λ point, which we identify with B_S. The data of Bowers[20] and of Kerrisk and Keller[21] cover the desired region and have been used in Fig. 10 to plot D_S vs T. From the minimum in the curve of Fig. 10 we infer

$$B_S = 2.0\times 10^{-4} \tag{5.7}$$

in units of cm^2/sec. Combined with Eq. (5.5), this yields

$$w_B = 0.5 , \tag{5.8}$$

which happens to be in good agreement with what we found in our recent two-loop study[10] of the precritical rise in D_S, for saturated vapor pressure (SVP).

From Eqs. (5.8) and (4.25) we obtain

$$c_s = 1 , \tag{5.9}$$

which has been used in Eq. (4.24) for the computation of w vs ln$x$ that is shown in Fig. 11 by the lower solid curve. The upper of the two dashed curves for W can be used as a basis for the computation of a first-order correction in w as discussed in Sec. IV D above. The upper solid curve and the lower dashed curve, both labeled NL, show w and W, respectively, for the nonlinear flow of Eqs. (4.31) and (4.32).

B. Quasiscaling exponent

The k-dependent effective scaling exponent for D_S is defined in Eq. (1.4). By means of Eq. (1.6) we put the k differentiation into the more convenient form

$$\frac{d}{d\ln k} = (1-x)\frac{d}{d\ln x} . \tag{5.10}$$

From Eqs. (1.7), (2.18), and (2.22) we have

$$D_S = (s/w)^{1/2} = (xw)^{-1/2} . \tag{5.11}$$

Substitution of Eqs. (5.11), (5.10), and (1.8) into Eq. (1.4) gives

$$z_{\mathrm{eff}} = -x + (1-x)\frac{d\ln w}{d\ln x} = -x + (1-x)W(w,x) . \tag{5.12}$$

We now limit our attention to the case $c=1$ and for the moment concentrate on $w^*=0$. Equations (2.34) and (2.43) thus give

$$W(w,x) = v(x)w = (1-x)w , \tag{5.13}$$

which, substituted into Eq. (5.12), yields

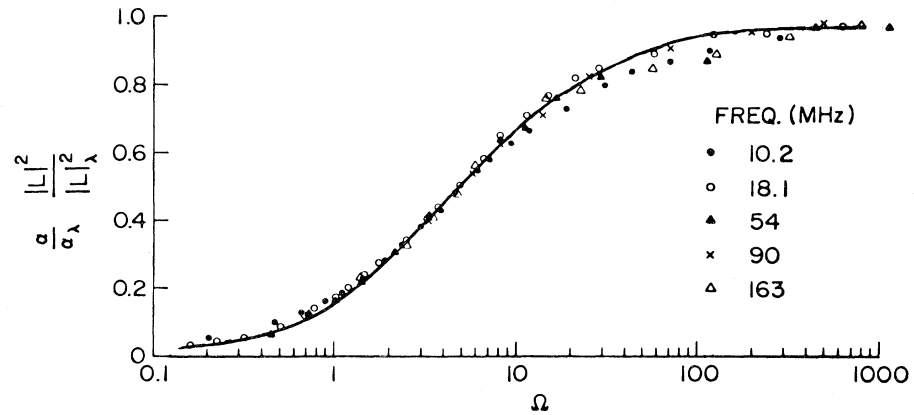

FIG. 9. Normalized ultrasonic attenuation data of Tozaki and Ikushima (Ref. 18) vs reduced frequency for five different frequencies. The fit of the scaled data to the theory (Ref. 17) determines the background kinetic coefficient $B_\psi = 1.0\times 10^{-4}$ cm^2/sec.

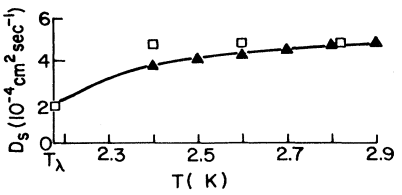

FIG. 10. Noncritical temperature dependence of the entropy diffusion coefficient D_S according to Bowers (Ref. 20) and Kerrisk and Keller (Ref. 21). The minimum value near the λ point is taken as the background parameter $B_S=2.0\times10^{-4}$ cm^2/sec.

$$z_{\text{eff}}=-x+(1-x)^2w \ . \tag{5.14}$$

This has a maximum at the quasiscaling point x_Q specified by

$$\frac{dz_{\text{eff}}}{dx}=0$$

$$=-1-2(1-x_Q)w+(1-x_Q)^2x_Q^{-1}w^2 \ , \tag{5.15}$$

where we have again made use of the flow equation. The root of this quadratic equation is

$$w=\frac{x_Q+\sqrt{x_Q}}{(1-x_Q)^2} \ , \tag{5.16}$$

which, substituted into Eq. (5.14), gives us the maximum value of z_{eff}, the quasiscaling exponent

$$z_Q=\sqrt{x_Q} \ . \tag{5.17}$$

The crossing of the curve for w vs x shown in Fig. 11 with that from Eq. (5.16) gives

$$w_Q=0.224 \tag{5.18a}$$

and

$$x_Q=0.032 \ , \tag{5.18b}$$

as noted by the downward pointing arrow in Fig. 11. Substituted into Eq. (5.17), Eq. (5.18a) yields

$$z_Q=0.18 \ , \tag{5.19}$$

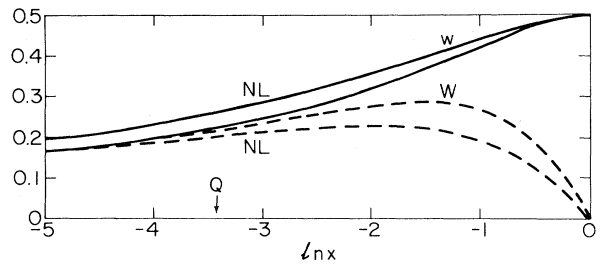

FIG. 11. Kinetic coefficient ratio w (solid curves) and flow function W (dashed curves) vs ln$x$, for the nonlinear flow function (outer curves labeled NL) and for the linear flow function (inner curves). The downward pointing arrow labeled Q indicates the location of the quasiscaling point.

which is smaller but not inconsistent with the roughly 20% enhancement of the slope of the log-log plot of D_S that we reported in Ref. 1. Comparison of the two dashed curves for W in Fig. 11 indicates that the nonlinear flow modification does not change appreciably the value of z_Q.

Figure 12 shows the kinetic coefficients $D_{\psi,S}$ obtained from the ratio w shown in Fig. 11. These curves are for $w_B=0.5$, as seen by the limiting ratio of $B_S/B_\psi=2$ at their right-hand ends. The lower curve, for D_ψ, can be used to extend the λ-point ultrasonic attenuation theory[17] out of the van Hove region and into the range of lower frequencies. Quasiscaling, as we have defined it, is a property only of the upper curve, for D_S. The quasiscaling point is shown at $k_Q=0.033$ by the solid circle marked Q. This is the point of inflection and the curve is straight in an interval of one and one-half decades in the vicinity of Q. It immediately follows that after conversion to zero frequency and then into the local limit, the log-log plot of the corresponding thermal-diffusion coefficient D_{SL} as a function of κ will have a corresponding straight section. In terms of temperature this means a straight run of more than two decades. Experimental measurements of D_{SL}, as they are extended toward the λ point, will show the van Hove precritical rise above B_S. When the rise in D_{SL} grows by 1 order of magnitude, the measurements will seem to be in the middle of a true scaling region, but with an exponent larger than expected from dynamic scaling by the factor $1+z_Q$. This is precisely what we mean by "quasiscaling."

With Eq. (5.19) and Fig. 12 we have achieved our primary goal: the establishment of the *quasi*scaling point and the calculation of the quasiscaling exponent, for the special case $w^*\simeq0$. This is our best current estimate of w^*. It is, however, entirely possible that higher-order contributions will make w^* negative. This would correspond in Fig. 3 to having the stability boundary pass above the physical point. The latter would then lie in the weak-scaling region. For this reason we give an estimate here of the w^* dependence of z_Q for the full interval $-1\le w^*\le0$. We begin with the derivative of $z_Q(w^*)$ evaluated at $w^*=0$. Because z_{eff} is at its maximum, we can neglect the effect of the variation of x_Q in Eq. (5.12) to find

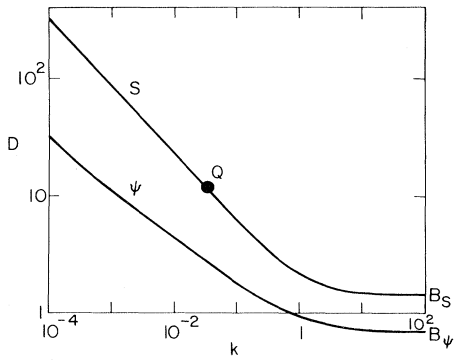

FIG. 12. Kinetic coefficients $D_{S,\psi}$ vs k for $w_B=0.5$. At the quasiscaling point, located by the solid dot labeled Q, the quasiscaling exponent $z_Q=0.18$ corresponds to a slope of the log-log plot 18% greater than expected from dynamic scaling.

$$\frac{dz_Q}{dw^*}=(1-x_Q)\left[\frac{\partial W}{\partial w^*}+\frac{\partial w}{\partial w^*}\frac{\partial W}{\partial w}\right]$$
$$=(1-x_Q)\left[-1+(1-x_Q)\frac{\partial w}{\partial w^*}\right]$$
$$\simeq -1+\frac{\partial w}{\partial w^*} \quad . \tag{5.20}$$

Here we continue to use $b=0$ and $c=1$. Because we have already located the quasiscaling point, the computation is now no longer as delicate as it was in Eq. (5.15). Therefore we have neglected x_Q compared to 1 in Eq. (5.20). From Eq. (4.15) (see also Appendix B) we have

$$\frac{\partial w^{-1}}{\partial w^*}=(w_B^{-1}-1)\ln x-1-\tfrac{1}{2}\ln^2 x+x \quad . \tag{5.21}$$

Neglecting the last term and substituting $w_B=0.5$, w_Q from Eq. (5.18a), and x_Q from Eq. (5.18b), we obtain

$$\frac{\partial w}{\partial w^*}=-w^2\frac{\partial w^{-1}}{\partial w^*}=(0.224)^2\times 10.4=0.52 \quad , \tag{5.22}$$

which, inserted into Eq. (5.20), gives

$$\frac{dz_Q}{\partial w^*}\simeq -0.48 \quad . \tag{5.23}$$

The first term of the right-hand member of Eq. (5.20) expresses the difference between the weak-scaling exponent and the standard (strong) dynamic scaling exponent. As w^* becomes negative the second term decreases rapidly. A convenient approximant for the w^* dependence of z_Q which adequately fits Eqs. (5.19) and (5.23) is

$$z_Q(w^*)=-w^*+0.18(1+w^*)^3 \quad , \tag{5.24}$$

as shown in Fig. 13 for $-1\leq w^*\leq 0$. In Appendix C an independent calculation confirms the accuracy of Eq. (5.24) at $w^*=-0.5$.

The effect on $D_{\psi,S}$ of varying w^* is illustrated in more detail in Fig. 8 by the lower (dashed) curves and the upper (solid curves), respectively. For convenience, the computations were carried out for $w_B=1$. The values $w^*=0$, -0.5, and -1 are indicated on the curves. For the case $w^*=0$, discussed above in Sec. IV, dynamic scaling has already broken down and there is no longer an asymptotic scaling region. $D_S/D_\psi=w^{-1}\to\infty$, and the pair of curves fans apart without limit as $k\to 0$. Quasiscaling occurs at $x_Q=0.060$ and $k_Q=0.064$ as indicated, and yields the quasiscaling exponent $z_Q=0.24$. The trend is accentuated for $w^*<0$, with the D_S curve steepening, the quasiscaling point receding toward smaller values of k, and z_Q steadily increasing. In Appendix B we find for $w_B=1$ and $w^*=-0.5$, $x_Q=0.028$, $k_Q=0.029$ (as noted in Fig. 8), and $z_Q=0.54$.

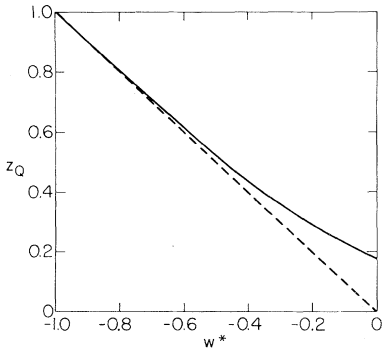

FIG. 13. Dependence of the quasiscaling exponent on the weak-scaling parameter w^*. The dashed staight line represents the asymptotic weak-scaling exponent. The solid curve shows the additional steepening of the log-log plot of D_S vs k that occurs at the quasiscaling point.

As explained above in Sec. II B, $w^*=-1$ occurs at the natural boundary of the SSS model (dashed line in Fig. 3). The curve for $w^*=-1$ forms therefore a natural limit for the family of curves in Fig. 8. At this boundary the entropy curve reaches its weak-scaling limit

$$D_S=\frac{1}{x}=\frac{1}{k}+1 \quad , \tag{5.25}$$

with double the (strong) dynamic scaling exponent.

The quasiscaling exponent attains its maximum value

$$z_Q(-1)=1 \quad . \tag{5.26}$$

This is the same trend that for $w_B=0.5$ is described by Eq. (5.24) and illustrated in Fig. 13.

C. Comparison with experiment

We are now ready to compare our theoretical prediction, as expressed by Eq. (5.19), with the experimental measurements. As mentioned in Sec. I, an inconsistency has recently been revealed in the experimental data by the report of differing thermal conductivities for different sized cells.[8] Since there is, as long as this discrepancy persists, no definitive experimental curve for the thermal conductivity λ versus the reduced temperature t, it follows that there obviously cannot be any definitive comparison of the theory with experiment. It will therefore suffice here simply to *illustrate* how this comparison is to be effected, leaving a more complete treatment to await clarification of the experimental situation. For the purpose of illustration we make use of some earlier measurements by Ahlers[22] of λ, as shown in the log-log plot of Fig. 14. It is apparent that λ rises monotonically as $t\to 0$, with an apparent straight, or quasiscaling portion developing close to the critical point, for the smallest values of t. From the slope in Fig. 14 it is possible to infer the value of the quasiscaling exponent z_Q, the fractional excess of the slope over its dynamic scaling value.

But in estimating the excess slope we must allow for the critical specific heat, which we regard as a nondynamical slowly varying parameter in the k-κ space of Fig. 1. Along the κ_+ axis ($k=0$), in the crossover and quasiscaling regions, the temperature dependence of the specific heat is expressed by a constant times

$$C(t)=\ln\frac{t_0}{t} \quad , \tag{5.27}$$

where t_0 is an empirical parameter of the order of 10^{-2}. With the location of the quasiscaling point estimated at $t_Q\simeq 10^{-5}$ we find from Eq. (5.27)

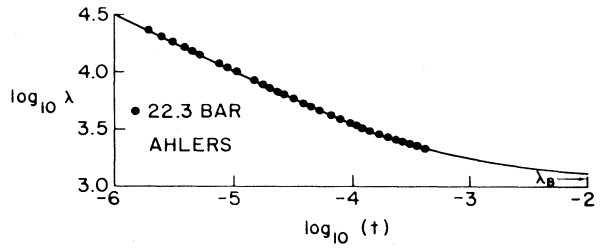

FIG. 14. Thermal conductivity vs reduced temperature, after Ahlers *et al.* (see Ref. 8). The right-hand end indicates the noncritical background value according to Kerrisk and Keller (Ref. 21). The slope of the straight line, or "quasiscaling" portion of the curve, yields the quasiscaling exponent, after appropriate account is taken of the critical specific heat.

$$C(t_Q)\simeq \ln 10^2 = 6.9 \ . \tag{5.28}$$

In the vicinity of t_Q, $C(t)$ can be described by a power of t with the exponent

$$\left.\frac{d\ln C(t)}{d\ln t}\right|_{t_Q} = -\frac{1}{C(t_Q)} \simeq -0.14 \ . \tag{5.29}$$

The dynamic scaling prediction for λ is the temperature dependence $t^{-1/3}$ times the square root of $C(t)$, corresponding to a total effective exponent of $-0.33 + (-0.07) \simeq -0.40$. This can be compared with the slope in Fig. 1, which is evidently -0.50. The fractional excess slope determines the quasiscaling exponent as

$$z_Q \simeq \frac{0.50-0.40}{0.40} = 0.25 \ . \tag{5.30}$$

Considering the provisional nature of the experimental data, this is in satisfactory agreement with the theoretical value 0.18 of Eq. (5.19), for SVP.

VI. DISCUSSION AND SUMMARY

The main qualitative feature of the critical dynamics of the λ transition is the existence of a slow transient which postpones almost indefinitely the onset of the true scaling region. This is a consequence of the smallness of the fixed-point value w^* of w, the ratio of the order parameter and entropy kinetic coefficients. The two-loop[11,12,4] ϵ expansion yields $w^* \simeq 0.1$. On the basis of velocity persistence[2,3] we expect w^* to be further reduced by the three-loop and higher-loop contributions. For this reason, and in the interest of simplicity, in writing this paper we have used the working hypothesis $w^*=0$. A possible deviation of w^* from zero is dealt with in Sec. V B and in Fig. 13. In this connection we are obliged at this point to take cognizance of the fact that in the paper of Ahlers, Hohenberg, and Kornblitt[8] the hypothesis $w^*=0$ is rejected. This rejection is, however, negated by their *Note added in proof.*

The main product of our paper is our very simple result for the kinetic coefficient ratio

$$w = \frac{D_\psi}{D_S} = \frac{1}{1+x-\ln x} \ , \tag{6.1}$$

where

$$x = \frac{k}{k+k_c} \ . \tag{6.2}$$

k_c is the characteristic wave number defined in Sec. II A. The two important limits are $k \to 0$, where $x \simeq k/k_c$ and $k \to \infty$ (the precritical and background region), where Eq. (6.2) reduces to

$$1-x = \frac{k_c}{k+k_c} \simeq \frac{k_c}{k} \ . \tag{6.3}$$

The salient properties of Eq. (6.1) can be enumerated as follows.

(a) $w \to w^* = 0$ as $k \to 0$.

(b) The approach to the fixed point $w^*=0$ is described by a transient.

(c) $dw/dx = 0$ as $k \to \infty$. According to Eq. (6.3) this implies a completely flat precritical behavior for w. In other words, as discussed in Sec. III A, w has zero precritical rise.

(d) Equation (6.1) provides a smooth and monotonic interpolation formula for w between the limits $k \to 0$ and $k \to \infty$.

(e) Equation (6.1) fixes the k dependence of the entropy kinetic coefficient. This exhibits quasiscaling with the quasiscaling exponent $z_Q = 0.18$. z_Q is stable with respect to the nonlinear modification of the flow equations. Although for a given k the value of w changes, the value of the flow function itself is relatively insensitive, leading to practically the same value for z_Q.

It is useful to compare our treatment and results with those of Dohm and Folk[7] and of Ahlers, Hohenberg, and Kornblitt[8].

(i) The quasiscaling behavior, which is the *Leitmotiv* of the present work, has gone largely unnoted in the above treatment,[7,8] perhaps because these authors express their results in terms of the so-called "universal amplitude ratio." This is a useful quantity in the scaling region. But the scaling region is experimentally unattainable and may not even exist. Thus we feel that the universal amplitude ratio is not a useful way to exhibit the results of the flow equations. Although no information is lost by using the universal amplitude ratio, it does tend to obscure the simple behavior of λ. The smooth and monotonic approach of λ toward its background value is transformed into a minimum in the universal amplitude ratio. At higher temperatures the flat noncritical background is converted into a spurious and artifical "critical behavior" of the universal amplitude ratio, proportional to $\kappa^{1/2}$.

(ii) By imposing the approximate proportionality for the product of the coefficients, $D_S D_\psi \propto x^{-1}$, we are able to reduce the general problem of the flow in two variables to a single differential equation involving only the one unknown $w = D_\psi / D_S$.

(iii) By studying the flow in k space we have a monotonic behavior for w. As discussed in Sec. III B, the κ-dependent flow used in the papers of Dohm and Folk[7] and of Ahlers, Hohenberg, and Kornblitt[8] necessarily brings in a nonmonotonic behavior of w as a function of k. This makes the interpolation between the "anchor" regions $k \to 0$ and $k \to \infty$ awkward and less reliable.

(iv) We evaluate the loop integrals in three dimensions. This is especially important in the precritical region where

the single-loop integral gives a rigorous solution to the problem. As noted in Sec. III B, the flow equation used by Ahlers, Hohenberg, and Kornblitt[8] seems to be inconsistent with this rigorous requirement.

(v) Contrary to the procedures employed by the other authors[7,8] all of our parameters are determined *a priori*. There are no free parameters to be adjusted to fit critical data for D_S. Furthermore, our phenomenological flow equation is flexible and can easily incorporate the contributions of the higher-loop integrals. The complete computer calculations are more specialized and less easy to adapt to changes in input.

In summary, we believe that the quasiscaling point and the quasiscaling exponent $z_Q \simeq 0.18$ contain the essence of the crossover problem that is encountered at the λ point of liquid ^{4}He. We contend that our phenomenological flow equation in wave-number space has many advantages and that it is sufficiently accurate to give insight into, as well as a quantitative account of, the quasiscaling behavior.

ACKNOWLEDGMENT

We are happy to acknowledge support from the National Science Foundation under Grants Nos. DMR-79-01172 and DMR-82-05356.

APPENDIX A: SINGLE-LOOP ENTROPY INTEGRAL

The precritical rise in the entropy diffusion coefficient is determined by the integral $I_S(\bar{\epsilon})$, as defined in Eq. (2.3). It is convenient to generalize this integral to the form

$$J_S(\bar{\epsilon},z)=\frac{1}{4\pi}\int \frac{d^3p}{p^2p'^2}\frac{(p^2-p'^2)^2}{p^{1+\bar{\epsilon}}+(p')^{1+\bar{\epsilon}}+z} , \tag{A1}$$

so that the desired integral is given by

$$I_S(\bar{\epsilon})=J_S(\bar{\epsilon},1) . \tag{A2}$$

The simpler zero-frequency integral is

$$\bar{I}_S(\bar{\epsilon})=J_S(\bar{\epsilon},0)=\frac{2}{3}\frac{1}{\bar{\epsilon}}+\frac{8}{9} , \tag{A3}$$

where the two-term $\bar{\epsilon}$ expression[12] can be tested at $\bar{\epsilon}=1$. Exact integration gives $\bar{I}_S=\pi/2=1.57$, while Eq. (A3) gives $\frac{14}{9}=1.56$, or 1% accuracy. (The $\bar{\epsilon}$ expansion is more accurate than the ϵ expansion because it does not have to contend with any infrared divergence.)

In the very-high-frequency range $z \gg 1$ the integration occurs predominately for $p \gg 1$ so that we can use the high-momentum approximation in Eq. (A1) to obtain

$$J_S(\bar{\epsilon},z)\simeq \tfrac{4}{3}\int_0^\infty \frac{dp}{2p^{1+\bar{\epsilon}}+z} = K(\bar{\epsilon})z^{-\bar{\epsilon}/(1+\bar{\epsilon})} , \tag{A4}$$

where

$$K(\bar{\epsilon})=\frac{2}{3}\frac{2^{\bar{\epsilon}/(1+\bar{\epsilon})}}{1+\bar{\epsilon}}\frac{\pi}{\sin[\pi\bar{\epsilon}/(1+\bar{\epsilon})]} . \tag{A5}$$

We therefore bridge between the two extreme limits of Eqs. (A3) and (A4) by the Padé approximant

$$J_S(\bar{\epsilon},z)\simeq\frac{\bar{I}_S(\bar{\epsilon})}{(1+\gamma z)^{\bar{\epsilon}/(1+\bar{\epsilon})}} , \tag{A6}$$

where

$$\gamma^{\bar{\epsilon}/(1+\bar{\epsilon})}=\frac{\bar{I}_S(\bar{\epsilon})}{K(\bar{\epsilon})} . \tag{A7}$$

The desired integral for frequency $z=1$ is obtained from Eqs. (A2) and (A6) as

$$I_S(\bar{\epsilon})\simeq\frac{\bar{I}_S(\bar{\epsilon})}{[1+\gamma(\bar{\epsilon})]^{\bar{\epsilon}/(1+\bar{\epsilon})}} . \tag{A8}$$

For $\bar{\epsilon}=1$ we have $\bar{I}_S(1)=1.556$, $K(1)=1.481$, and $\gamma(1)=1.103$, so that Eq. (A8) gives

$$I_S(1)\simeq 1.07 , \tag{A9}$$

as reported in Sec. II A following Eq. (2.5).

We can check the accuracy of Eq. (A6) for $\bar{\epsilon}=1$ by calculating the zero-frequency derivative

$$-\frac{\partial J_S(1,0)}{\partial z}\simeq\frac{\gamma(1)}{2}\bar{I}_S(1)=0.858 . \tag{A10}$$

Exact evaluation by elliptical coordinates gives

$$-\frac{\partial J_S(1,0)}{\partial z}=\frac{1}{4\pi}\int\frac{d^3p(p^2-p'^2)}{p^2p'^2(p^2+p'^2)^2} =\frac{\pi}{2}\left[\frac{\pi}{2}-1\right]=0.897 , \tag{A11}$$

showing that (A10) is 4% too low. This can be adjusted by raising $\gamma(1)$ by 4%, which, however, has only a 1% effect on Eq. (A8). This correction is cancelled by raising $\bar{I}_S(\bar{\epsilon})$ to its exact value. Therefore we believe that Eq. (A9) is accurate to within 1%, which we in fact have verified by numerical integration.

The same computation can also be readily carried out for the scaling region, where $\bar{\epsilon}=\frac{1}{2}$. Then $\bar{I}_S(\frac{1}{2})=\frac{20}{9}=2.222$, $K(\frac{1}{2})=2.031$, and $\gamma(\frac{1}{2})=1.309$, so that Eq. (A6) yields

$$I_S(\tfrac{1}{2})\simeq 1.68 .$$

The value of 1.92 which we have previously reported[12] for this integral we now believe to be in error. Numerical integration gives $I_S(\frac{1}{2})\simeq 1.70$.

APPENDIX B: WEAK SCALING

We provide here the details of the solution of the flow equation for weak scaling, where $w^*<0$. In this case w^* is not the fixed-point value of w but is instead the exponent in the asymptotic behavior

$$1/w(x)\sim x^{w^*}=x^{-|w^*|} \tag{B1}$$

as $x\to 0$. The individual kinetic coefficients behave consequently as

$$D_\psi=\sqrt{sw}\sim x^{-1/2(1+w^*)} \tag{B2}$$

and

$$D_S=\sqrt{s/w}\sim x^{-1/2(1-w^*)} . \tag{B3}$$

The proportionality coefficient in Eq. (B1) is found from

Eq. (4.15) to be

$$c_w=\frac{1}{w_B}e^{-b}+\int_0^1\frac{dx}{x^{1+w^*}}e^{-bx}-c\int_0^1\frac{dx}{x^{w^*}}e^{-bx} \quad . \tag{B4}$$

Restricting ourselves now to $b=0$ and $c=1$ this reduces to

$$c_w=w_B^{-1}-(w^*)^{-1}-(1-w^*)^{-1} \quad . \tag{B5}$$

The full solution from Eq. (4.15) is

$$w^{-1}=c_w x^{w^*}+(w^*)^{-1}+(1-w^*)x \quad , \tag{B6}$$

which was used in calculating the curves in Fig. 8.

From Eq. (B6) we obtained Eq. (5.21) for $\partial w^{-1}/\partial w^*$, which we used for calculating dz_Q/dw^* at $w^*=0$. To determine $z_Q(w^*)$ for finite $|w^*|$ we can still use Eq. (5.12), where, however, we now have $u=w^*$ so that the flow function is

$$W(w,x)=-w^*+(1-x)w \quad . \tag{B7}$$

Including the additional terms in Eq. (5.14) yields

$$\begin{aligned} z_{\text{eff}}&=w^*-(1-w^*)x+(1-x)^2w \\ &\simeq -w^*-(1-w^*)x+w \quad , \end{aligned} \tag{B8}$$

where the small-x approximation in the last term is valid for sufficiently large $|w^*|$, i.e., $|w^*|\geq 0.5$). The quasiscaling point is to be found by differentiating Eq. (B8):

$$\begin{aligned} \frac{dz_{\text{eff}}}{dx}=0&=-(1-w^*)+\frac{dw}{dx} \\ &=-1+w^*+\frac{w}{x}W \\ &\simeq -1+w^*-w^*\frac{w}{x} \quad . \end{aligned} \tag{B9}$$

On substituting Eq. (B7) we have dropped the small second term. Equation (B9) gives the desired relationship

$$w_Q=\left[1-\frac{1}{w^*}\right]x_Q \quad , \tag{B10}$$

which, substituted into Eq. (B8), yields the quasiscaling exponent

$$z_Q\simeq -w^*+\left[w^*-\frac{1}{w^*}\right]x_Q \quad . \tag{B11}$$

This approximation, which is not valid for small $|w^*|$, supplants Eq. (5.17), which holds only at $w^*=0$.

We now apply the above equations to the specific case $w^*=-\frac{1}{2}$. Equations (B11) and (B10) become

$$z_Q=\tfrac{1}{2}+\tfrac{3}{2}x_Q \tag{B12}$$

and

$$w_Q=3x_Q \quad . \tag{B13}$$

For Eq. (B4) we have

$$c_w=w_B^{-1}+\tfrac{4}{3} \tag{B14}$$

so that Eq. (B6) reads

$$w^{-1}\simeq(w_B^{-1}+\tfrac{4}{3})x^{-1/2}-2 \quad , \tag{B15}$$

where we have dropped the term $2x/3$. The simultaneous solution of Eqs. (B13) and (B15) is the root of the quadratic equation

$$6x_Q-\left[4+\frac{3}{w_B}\right]\sqrt{x_Q}+1=0 \quad . \tag{B16}$$

For $w_B=1$ we find $\sqrt{x_Q}=\frac{1}{6}$, so $x_Q=\frac{1}{36}$, $k_Q=\frac{1}{35}$ (as indicated in Fig. 8), and $z_Q=0.54$. $w_B=0.5$ yields $k_Q\simeq x_Q=(5+\sqrt{19})^{-2}=0.011$ and

$$z_Q(-\tfrac{1}{2})\simeq 0.52 \quad , \tag{B17}$$

in support of Eq. (5.24).

Before closing this study we are obliged to deal with a minor inconsistency. In the above we have held $c=1$, which runs counter to the natural boundary limit $W=1$ [Eq. (2.12)]. The latter requires $c=0$ and $b=w_B$ [from Eq. (2.47)]. A w^* dependence consistent with this limit would be

$$c=1+w^* \tag{B18a}$$

and

$$b=-w^*w_B \quad , \tag{B18b}$$

which satisfies Eq. (2.47).

For $w^*=-\frac{1}{2}$ and $w_B=\frac{1}{2}$ we should therefore be using $b=\frac{1}{4}$ and $c=\frac{1}{2}$, instead of $b=0$ and $c=1$. Returning to the general solution, by an integration by parts we put Eq. (4.15) into the form

$$\begin{aligned} w^{-1}=&[w_B^{-1}-(w^*)^{-1}]x^{w^*}e^{-b(1-x)}+(w^*)^{-1} \\ &-\left[\frac{b}{w^*}+c\right]e^{bx}\int_x^1\frac{dx'}{(x')^{w^*}}e^{-bx'} \quad . \end{aligned} \tag{B19}$$

The incomplete Γ function can be expressed in terms of the error function for $w^*=-\frac{1}{2}$. But the coefficient is, by Eqs. (18a) and (18b),

$$\frac{b}{w^*}+c=1+w^*-w_B \quad , \tag{B20}$$

which happens to vanish (an unexpected but pleasant occurrence) for the case of interest. Thus the substitution of $w^*=-\frac{1}{2}$, $w_B=\frac{1}{2}$, and $b=\frac{1}{4}$ into Eq. (B19) yields

$$w^{-1}=c_w x^{-1/2}e^{-x/4}-2 \quad , \tag{B21}$$

where

$$c_w=4e^{-1/4}=3.12 \quad . \tag{B22}$$

This is down by only 3% from the value

$$c_w=\tfrac{10}{3}=3.33 \tag{B23}$$

given by Eq. (B14) above. It is thus evident that the in-

consistency in adhering to $c=1$, dictated solely by convenience, produces a negligible error in Eq. (B17). We find a larger but still minor effect on $\partial w/\partial w^*$. If we include in Eq. (5.21) the additional terms coming from differentiating b and c in Eq. (5.19), as required by Eqs. (18a) and (18b) we find Eq. (5.22) increased from 0.52 to 0.60, and dz_Q/dw^* in Eq. (5.23) changed from -0.48 to -0.40. This change is small enough that we can still regard Eq. (5.24) and Fig. 13 as a fair representation of the w^* dependence of z_Q.

---

*Present address: Department of Physics, Indian Institute of Technology, Kanpur 208016, India.

[1]R. A. Ferrell and J. K. Bhattacharjee, Phys. Rev. Lett. 42, 1638 (1979).

[2]R. A. Ferrell and J. K. Bhattacharjee, in *Proceedings of the International Conference on Critical Dynamics, Geneva, 1979,* edited by C. P. Enz (Springer, Berlin, 1979).

[3]R. A. Ferrell and J. K. Bhattacharjee, in *Light Scattering in Solids,* edited by J. Birman, H. Z. Cummins, and K. K. Rebane (Plenum, New York, (1979); R. A. Ferrell and J. K. Bhattacharjee, Phys. Rev. B 20, 3690 (1979).

[4]R. A. Ferrell and J. K. Bhattacharjee, J. Low Temp. Phys. 36, 184 (1979).

[5]P. C. Hohenberg, B. I. Halperin, and D. R. Nelson, Phys. Rev. B 22, 2373 (1980).

[6]V. Dohm and R. Folk, Z. Phys. B 40, 79 (1980).

[7]V. Dohm and R. Folk, Phys. Rev. Lett. 46, 349 (1981); Z. Phys. B 41, 251 (1981); 45, 129 (1981). See also V. Dohm and R. Folk, Physica 109 & 110B, 1549 (1981).

[8]G. Ahlers, P. C. Hohenberg, and A. Kornblit, Phys. Rev. Lett. 46, 493 (1981); Phys. Rev. B 25, 3136 (1982).

[9]J. K. Bhattacharjee and R. A. Ferrell, Physica 107B, 341 (1981).

[10]J. K. Bhattacharjee and R. A. Ferrell, Phys. Rev. B 25, 216 (1982).

[11]L. Sasvari, F. Schwabl, and P. Szépfalusy, Physica 81A, 108 (1975).

[12]J. K. Bhattacharjee and R. A. Ferrell, J. Math. Phys. 21, 534 (1980).

[13]C. DeDominicis and L. Peliti, Phys. Rev. Lett. 38, 505 (1977); Phys. Rev. B 18, 353 (1978).

[14]V. Dohm and R. A. Ferrell, Phys. Lett. 67A, 387 (1978).

[15]J. K. Bhattacharjee, M. S. Korth, and R. A. Ferrell (unpublished).

[16]K. Kawasaki and J. Gunton, Phys. Rev. B 13, 4658 (1976).

[17]R. A. Ferrell and J. K. Bhattacharjee, Phys. Rev. Lett. 44, 403 (1980).

[18]K. Tozaki and A. Ikushima, J. Low. Temp. Phys. 32, 379 (1978).

[19]R. A. Ferrell and J. K. Bhattacharjee, Phys. Rev. B 25, 3168 (1982).

[20]R. Bowers, Proc. Phys. Soc. London Sect. A 65, 511 (1952).

[21]J. Kerrisk and W. E. Keller, Phys. Rev. 177, 341 (1969).

[22]See Ref. 8 for a guide to the experimental literature.